Z. Phys. C – Particles and Fields 52, 361–387 (1991)

Zeitschrift für Physik C Particles and Fields

Forward produced hadrons in μp and μd scattering and investigation of the charge structure of the nucleon

European Muon Collaboration

J. Ashman[12], B. Badelek[15,a], G. Baum[17,b], J. Beaufays[2,c], C.P. Bee[7], C. Benchouk[8], I.G. Bird[4,d], S.C. Brown[7,e], M.C. Caputo[17,f], H.W.K. Cheung[10,g], J.S. Chima[11,h], J. Ciborowski[15,a], R. Clifft[11], G. Coignet[6], F. Combley[12], G. Court[7], G. d'Agostini[8], J. Drees[16], M. Düren[4], N. Dycew[5], A.W. Edwards[16,i], M. Edwards[11], T. Ernst[3], J. Favier[6], M.I. Ferrero[13], D. Francis[7], E. Gabathuler[7], R. Gamet[7], V. Gibson[10,j], J. Gillies[10,k], P. Grafström[14,j], K. Hamacher[16], D. von Harrach[4,l], P. Hayman[7], J.R. Holt[7], V.W. Hughes[17], A. Jacholkowska[2,m], T. Jones[7,k], E.M. Kabuss[4,l], B. Korzen[16], U. Krüner[16], S. Kullander[14], U. Landgraf[3], D. Lanske[1], D. Lauterjung[16], F. Lettenström[14,n], T. Lindqvist[14], J. Loken[10], M. Matthews[7], Y. Mizuno[4,o], K. Mönig[16], F. Montanet[8], E. Nagy[6,p], J. Nassalski[15,q], T. Niinikoski[2], P.R. Norton[11], F.G. Oakham[11,r], R.F. Oppenheim[17,s], A.M. Osborne[2], V. Papavassiliou[17], N. Pavel[16,t], C. Peroni[13], H. Peschel[16,u], R. Piegaia[17,f], B. Pietrzyt[8], U. Pietrzyk[16,v], B. Povh[4], P. Renton[10], J.M. Rieubland[2], K. Rith[4], E. Rondio[15,a], L. Ropelewski[15,a], D. Salmon[12,k], A. Sandacz[15,q], A. Schlagböhmer[3,w], A. Schneider[16], T. Schröder[3], K.P. Schüler[17], K. Schultze[1], T.-A. Shibata[4], T. Sloan[5], A. Staiano[13], H.E. Stier[3], J. Stock[3], G.N. Taylor[10,x], J.C. Thompson[11], T. Walcher[4,l], J. Toth[6,p], L. Urban[1], L. Urban[6,p], H. Wahlen[16], W. Wallucks[3], M. Whalley[12,z], S. Wheeler[12,k], W.S.C. Williams[10], S.J. Wimpenny[7,z], R. Windmolders[9], J. Womersley[10,z'], K. Ziemons[1]

[1] III Physikalisches Institut A, Physikzentrum, RWTH, W-5100 Aachen, Federal Republic of Germany
[2] CERN, CH-1211 Geneva 23, Switzerland
[3] Fakultät für Physik, Universität Freiburg, W-7800 Freiburg, Federal Republic of Germany
[4] Max-Planck Institute for Kernphysik, W-6900 Heidelberg, Federal Republic of Germany
[5] Department of Physics, University of Lancaster, Lancaster LA1 4YB, UK
[6] Laboratoire d'Annecy-le-Vieux de Physique des Particules, B.P. 110, F-74941 Annecy-le-Vieux, Cedex, France
[7] Department of Physics, University of Liverpool, Liverpool L69 3BX, UK
[8] Centre de Physique des Particules, Faculté de Sciences de Luminy, F-13288 Marseille, France
[9] Faculté de Sciences, Université de Mons, B-7000 Mons, Belgium
[10] Nuclear Physics Laboratory, Unversity of Oxford, Oxford OX1 3RH, UK
[11] Rutherford and Appleton Laboratory, Chilton, Didcot OX1 0QX, UK
[12] Department of Physics, University of Sheffield, Sheffield S3 7RH, UK
[13] Istituto di Fisica, Università di Torino, I-10125, Italy
[14] Department of Radiation Science, University of Uppsala, S-75121 Uppsala, Sweden
[15] Physics Institute, University of Warsaw and Institute for Nuclear Studies, PL-00681 Warsaw, Poland
[16] Fachbereich Physik, Universität Wuppertal, W-54600 Wuppertal, Federal Republic of Germany
[17] Physics Department, Yale University, New Haven, CT 06520 USA

Received 14 March, 1991; in revised form 7 August, 1991

[a] University of Warsaw, Poland, partly supported by CPBP.01.06
[b] Permanent address, University of Bielefeld, Bielefeld, FRG
[c] Now at TRASYS, 1040 Brussels, Belgium
[d] Now at NIKHEF-K, 1009 AJ Amsterdam, The Netherlands
[e] Now at TESA S.A., Renens, Switzerland
[f] Now at City University, 1428 Buenos Aires, Argentina
[g] Now at University of Colorado, Boulder, CO 80302, USA
[h] Now at British Telecom, London, UK
[i] Now at Jet, Joint Undertaking, Abingdon, UK
[j] Now at CERN, Geneva, Switzerland
[k] Now at R.A.L., Chilton, Didcot, UK
[l] Now at University of Mainz, Mainz, FRG
[m] Now at L.A.L., Orsay, France
[n] Now at University of California, Santa Cruz, CA 950-64, USA
[o] Now at RCNP, Osaka University, Ibaraki, Osaka, Japan
[p] Permanent address, Central Research Institute for Physics, Hungarian Academy of Science, Budapest, Hungary
[q] Institute for Nuclear Studies, Warsaw, Poland, partly supported by CPBP.01.09
[r] Now at NRC, Ottawa, Canada
[s] Now at AT&T, Bell Laboratories, Naperville, Illinois, USA
[t] Now at DESY and University of Hamburg, II Institute of Experimental Physics, FRG
[u] Now at Gruner & Jahr, Itzehoe, FRG
[v] Now at MPI for Neurologische Forschung, Köln, FRG
[w] Now at GEI, Darmstadt, FRG
[x] Now at University of Melbourne, Parkville, Victoria, Australia
[y] Now at University of Durham, Durham, UK
[z] Now at University of California, Riverside, USA
[z'] Now at University of Florida, Gainesville, USA

Abstract. Final data measured with the EMC forward spectrometer are presented on the production of forward charged hadrons in μp and μd scattering at incident beam energies between 100 and 280 GeV. The large statistic of 373000 events allows a study of the semi-inclusive hadron production as a function of z, p_T^2 and $\langle p_T^2 \rangle$ in small Q^2, x_{Bj} and W bins. Charge multiplicity ratios and differences as a function of z and x_{Bj} are given for p, d and n-targets. From the differences of charge multiplicities the ratio of the valence quark distributions of the proton $d_v(x)/u_v(x)$ is determined for the first time in charged lepton scattering. The Gronau et al. sum rule is tested, the measured sum being 0.31 ± 0.06 stat. $\pm$ 0.05 syst., compared with the theoretical expectation of $2/7 \approx 0.286$. The measured sum corresponds to an absolute value of the ratio of the d and u quark charge of 0.44 ± 0.10 stat. ± 0.08 syst.

1 Introduction

During the period 1977 to 1985 the European Muon Collaboration (EMC) took data to perform a detailed series of measurements of deep inelastic muon nucleon scattering. In these experiments both the scattered muons and the hadronic final states have been measured. The NA2 (NA2′) phase of the experiment in 1977–1980 (1983–1985) concentrated on high statistics measurements of forward produced hadrons in addition to measurements of inclusive muon scattering. The NA9 phase (1981–1982) also included the backward region and provided powerful particle identification. This paper presents final results on the semi-inclusive distributions of forward produced charged hadrons from the NA2 and NA2′ phase for muon scattering from proton and deuteron targets. It is based on 154000 events from μp-scattering and 219000 events from μd-scattering. The incident beam energies were 120, 200 and 280 GeV for the μp- and 100 and 280 GeV for the μd-scattering. The large statistics available from these measurements enable detailed studies of the hadronic final states in small kinematic bins and allow detailed comparisons between the two targets.

Forward produced hadrons are the key to understand the fragmentation of the struck quark (current fragmentation). High statistical and systematic precision of the data is needed to measure subtile QCD effects such as scaling violations and factorisation breaking of the scaled energy distributions, especially because these effects are further distributed by residual target mass effects. Another, probably more direct, access to QCD effects is via the study of the transverse momentum p_t of the produced hadrons. Here charged lepton scattering experiments have the advantage with respect to e^+e^- annihilation that the reference direction of the process, the virtual photon direction, is directly measured. However, the study of QCD effects in p_t spectra is complicated by the intrinsic transverse momentum of the quarks inside the nucleon and by a contribution usually assigned to the (nonperturbative) fragmentation process. Therefore precise measurements of the kinematic dependences are needed to determine the dominant variables and to disentangle the contributions from the different sources.

As leading hadrons predominantly contain the struck quark, information about the quark (charge) composition of the nucleon can be obtained from their distributions. The data allow a study of this aspect in a large range of x_{Bj}; superior to those of previous experiments. Comparison of data on muon scattering from protons and deuterons gives information on the charge structure of the neutron. The ratio of the valence quark distributions of the proton $d_v(x)/u_v(x)$ can also be determined from this comparison. These data are complementary to neutrino scattering data and give important input and constraints to phenomenological quark distribution and structure function parameterisations needed for the analysis of hadron collider data. Finally, a sum rule derived by Gronau, Ravndal, and Zarmi [1], which is related to the (square of the) ratio of the u and d quark charge, can be tested. Using the measurement of the average squared valence quark charge from the comparison of the muon-nucleon and neutrino-nucleon structure functions, the absolute charges of the u and d quarks can be determined.

This paper is organised as follows:

In Sect. 2 we give briefly definitions of the variables and cross-sections. We describe how neutron rates have been extracted and introduce some other theoretical aspects.

Section 3 describes the apparatus, target setups, data analysis, and data sets, as well as cuts and corrections applied to the data. Sources of systematic errors are discussed and final systematic errors for semi-inclusive cross-sections and $\langle p_t^2 \rangle$ are given.

Section 4 contains the physics results. First we present semi-inclusive scaled energy and transverse momentum distributions of charged hadrons. Here we restrict ourselves mainly to the presentations of final data and do not repeat the detailed analysis presented in several previous papers [2]. The complete presentation of the data allows versatile phenomenological studies, fitting of models etc. Then charge multiplicity ratios for protons, deuterons and neutrons are discussed in detail. The differences of charge multiplicities are shown and the ratio of the $d_v(x)/u_v(x)$ valence quark distributions are extracted. Finally we present the first significant test of the Gronau et al. sum rule and the determination of the quark charges. The latter two subsections also include the necessary formulae, their derivation and a detailed discussion of the systematic errors.

In Sect. 5 we give a brief summary of the results of this paper.

2 Definition of variables and cross-sections

Throughout this paper we use standard variables relevant to deep inelastic scattering [3] which are $Q^2(\nu)$, the virtual photon squared four momentum (energy) transfer; x_{Bj} or simply x, the Bjorken scaling variable; y, the fraction of the muon energy transfer in the labora-

tory frame; and W^2, the mass squared of the hadronic system recoiling against the muon; i.e.:

$$Q^2 = -q^2 = -(k-k')^2 \cong 4EE' \sin^2 \frac{\Theta}{2},$$

$$\nu = \frac{q \cdot P}{M} = E - E',$$

$$x = \frac{Q^2}{2M\nu},$$

$$y = \frac{q \cdot P}{k \cdot P} = \frac{\nu}{E},$$

$$W^2 = (p+q)^2 = M^2 + 2M\nu - Q^2.$$

$k(k')$, $E(E')$ are the four momenta and energies of the incoming (scattered) muon respectively. P and M are the four momentum and mass of the target nucleon and Θ is the muon scattering angle in the laboratory frame. To describe the hadron kinematics we use the scaled hadron energy

$$z = \frac{P \cdot h}{P \cdot q} = \frac{E_h}{\nu},$$

and the square of the hadron transverse momentum with respect to the direction of the virtual photon, p_t^2, where h is the four momentum of the hadron and E_h its energy.

In the quark-parton model (QPM) the structure function of the nucleon can be expressed as

$$F_2^N(x) = x \cdot \sum_{i=u,d,\ldots} e_i^2 \, q_i(x),$$

where e_i are the quark charges and $q_i(x)$ the quark distribution functions; the probability densities to observe a quark i with momentum fraction x inside the nucleon. They obey relationships due to isospin and charge conjugation symmetries. For the distributions of the valence quarks, which define the quantum numbers of the nucleon, the following hold:

$$u_v(x) := u_{\text{valence}}^{\text{proton}}(x) = d_{\text{valence}}^{\text{neutron}}(x);$$
$$d_v(x) := d_{\text{valence}}^{\text{proton}}(x) = u_{\text{valence}}^{\text{neutron}}(x).$$

Further, the distribution of each type of sea quark is identical with that of its anti-quark partner inside the nucleon, so that in total the sea quarks carry the quantum numbers of the vacuum.

The naive QPM assumes independence of the actual virtual photon quark scattering and the fragmentation of the struck quark. Thus, if $D_i^h(z)$ is the probability density that a quark of type i fragments into a hadron h with energy fraction z, the normalised scaled energy distribution can be described as

$$\frac{1}{\sigma_{\text{tot}}} \cdot \frac{\mathrm{d}\sigma_h}{\mathrm{d}z} = \frac{1}{N_\mu} \cdot \frac{\mathrm{d}N_h}{\mathrm{d}z} = \frac{\sum_{i=u,d,\ldots} e_i^2 \, q_i(x, Q^2) \cdot D_i^h(z, Q^2)}{\sum_{i=u,d,\ldots} e_i^2 \, q_i(x, Q^2)}, \quad (1)$$

where N_μ denotes the number of events and N_h the number of hadrons.

This equation also holds in QCD in the leading log approximation. The explicitly written Q^2 dependence is due to QCD scaling violations of either the quark distributions or fragmentation functions. Higher order terms such as vertex corrections lead, in principle, to an x dependence of the fragmentation functions, thus to a (small) breaking of the factorising QPM ansatz.

Following the basic idea of the QPM we choose to present all hadron cross-sections as normalised differential cross-sections as a function of z or p_t^2. To show dependences on p_t^2 and z simultaneously, we present $\frac{1}{N_\mu} \cdot \frac{\mathrm{d}N_h}{\mathrm{d}p_t^2}$ in z bins. Previous studies of the azimuthal angle distribution in this experiment [4] have shown that it can be understood in terms of the QPM and QCD. Hence all distributions have been integrated over the azimuthal angle.

We do not show results on the characteristics of event shapes, like Thrust, Sphericity, $p_t^{\text{in}}/p_t^{\text{out}}$ as the apparatus acceptance is limited to the forward region and thus, only a small part of the tracks can be used to determine such quantities. We refer to results of previous analyses of the EMC [5].

For the derivation of the hadron production rates from neutrons we assumed that scattering from the deuteron takes place incoherently off the proton and neutron, because the deuteron is a weakly bound nuclear system (binding energy ~ 2.2 MeV). Apart from Fermi motion no evidence for other nuclear effects has been observed so far [6]. The corrections for Fermi smearing have been computed [7] and the influence on the hadron production rates was found to be less than 0.5% in the region $x < 0.5$ and has therefore been neglected. The hadron production rates from neutrons have been derived by subtracting the proton rate from the deuteron rate weighted by the cross section ratio equal to $F_2^n(x)/F_2^p(x)$.

$$\frac{1}{N_\mu^n} \frac{\mathrm{d}N^n}{\mathrm{d}z} = \left(1 + \frac{F_2^p}{F_2^n}\right) \frac{1}{N_\mu^d} \frac{\mathrm{d}N^d}{\mathrm{d}z} - \frac{F_2^p}{F_2^n} \cdot \frac{1}{N_\mu^p} \frac{\mathrm{d}N^p}{\mathrm{d}z}. \quad (2)$$

$F_2^n(x)/F_2^p(x)$ was taken from a linear parameterisation of the EMC data [7]. This ratio has been well measured by different experiments (see [8, 9] for a summary). A comparison, especially with the new precise measurement of the NMC [9], shows that an x dependent error of 5–10% covers the systematic uncertainty of this parameterisation for the applied range in x.

The measurement of the structure functions in deep inelastic charged lepton nucleon scattering cannot provide direct information about valence quark distributions. Through $F_2^n(x)/F_2^p(x)$ one can obtain information about the ratio of the distributions of all d and u quarks inside the proton, neglecting $s\bar{s}$ and heavier quarks,

$$\frac{d(x)}{u(x)} = \frac{1 - 4 \cdot (F_2^n(x)/F_2^p(x))}{(F_2^n(x)/F_2^p(x)) - 4}. \quad (3)$$

For high x this reflects the ratio of the valence quark distributions $d_v(x)/u_v(x)$, which in this region is less than 1/2 and decreases as x increases. For small x, however, the sea significantly contributes to the cross section. The

additional measurement of the hadronic final state provides a possibility to separate that part of the cross section originating from the sea, so that a direct measurement of $d_v(x)/u_v(x)$ becomes possible. In terms of the standard ideas on quark fragmentation, the hadron produced at the largest values of z will most likely contain the struck quark. Hence the charge and z dependence of the energy distributions are sensitive to the flavour of the fragmenting quark [10]. The difference of the normalised scaled energy distributions for positive and negative particles does not depend on sea quark, but only on valence quark distributions. Starting from (1), and using relations between fragmentation functions and between quark distribution functions, it is evident that the ratio $d_v(x)/u_v(x)$ can be extracted by constructing ratios of differences of charge multiplicities obtained from scattering from protons and neutrons. Explicitly we give the formulae in Sect. 4.4.

3 Experiment, data and analysis

The experiment was performed in the M2 muon beam line at the CERN SPS using the EMC forward spectrometer to detect the scattered muons and the fast forward hadrons. The data were taken in 11 experimental runs with incident muon energies of 100, 120, 200 and 280 GeV. The data sample consists of two parts, data taken in 1978/79 with a hydrogen target and in 1985 with a combined deuterium/copper target. The apparatus and target for the hydrogen data is described in detail elsewhere [11, 12]. The forward spectrometer for the 1985 data was similar to that described in [11], but modified to allow data to be taken at higher incident beam intensities [13]. The combined deuterium/copper target was designed to study the EMC effect [14] in detail, but for this analysis only events with a reconstructed vertex inside the liquid deuterium targets have been used. A comparison between the hadronic distributions from μd- and μCu-scattering can be found in [15].

The data were passed through a chain of analysis programs, in which pattern recognition and geometrical reconstruction of the incident and scattered muon as well as any charged hadron, which passed through the forward spectrometer, was performed. A vertex fit using the incident and scattered muons and hadrons was also performed. The vertex resolution is such that the individual targets can be clearly separated. Details of the hydrogen data analysis can be found in [16] and for the deuterium analysis in [17]. Although the reconstruction and analysis programs for the two data sets are different due to the large time gap, the philosophy of data reconstruction and analysis is almost the same.

For the track and event selection kinematical cuts (see Table 1) have been applied to both data sets. They were chosen to avoid regions where smearing, due to resolution and radiative effects, was large or where the acceptance was small or varied rapidly. This leaves for the hydrogen data set 154000 events and 219000 events for the deuterium data set, both covering the same kinematic range (see Table 2). A track is considered to belong

Table 1. Kinematic cuts for the data

Event selection			
$0.2<y<0.8$	$Q^2>2$ GeV^2	$\theta_{\mu'}>17$ mrad	for $E_\mu=100$ GeV
$0.2<y<0.8$	$Q^2>3$ GeV^2	$\theta_{\mu'}>17$ mrad	for $E_\mu=120$ GeV
$0.2<y<0.8$	$Q^2>4$ GeV^2	$\theta_{\mu'}>15$ mrad	for $E_\mu=200$ GeV
$0.2<y<0.8$	$Q^2>5$ GeV^2	$\theta_{\mu'}>14$ mrad	for $E_\mu=280$ GeV
Track selection			
$z_{had}>0.1$	$p_{had}>2$ GeV		for $E_\mu=100$ GeV
$z_{had}>0.1$	$p_{had}>2$ GeV		for $E_\mu=120$ GeV
$z_{had}>0.1$	$p_{had}>3$ GeV		for $E_\mu=200$ GeV
$z_{had}>0.1$	$p_{had}>5$ GeV		for $E_\mu=280$ GeV

Table 2. SPS periods and number of deep inelastic events after selection

SPS period	Target	Energy	Data	MC
P3A85	D_2	100 GeV	92000	150000
P3B85	D_2	100 GeV	60000	75000
P3B85	D_2	280 GeV	24000	22000
P3C85	D_2	280 GeV	43000	112000
Number of events d-target:			219000	359000
P3B279	H_2	120 GeV	24000	35000
P3A179	H_2	200 GeV	10000	49000
P3A279	H_2	200 GeV	23000	71000
P3B179	H_2	200 GeV	20000	83000
P4A79	H_2	280 GeV	17000	32000
P4B79	H_2	280 GeV	24000	35000
P8B78	H_2	280 GeV	36000	45000
Number of events p-target:			154000	350000

to an event, if its distance of closest approach to the vertex formed from the incoming and scattered muons is compatible with its error [16, 17]. For all data the acceptance of the apparatus was calculated from a complete Monte Carlo simulation using the Lund string model [18–20] to simulate the fragmentation processes. For the p_t^2-distribution, where the agreement between data and Monte Carlo was unsatisfactory the Monte Carlo tracks have been reweighted in an iterative procedure to follow data. Radiative effects due to QED processes have been included in the simulation [21] as well as secondary interactions of the produced particles in the target material. The scattered muon and the produced hadrons were tracked through the spectrometer taking into account the effects of multiple coulomb scattering. For the analysis of the deuterium data secondary interactions of all particles inside the spectrometer material have also been simulated. The effects of hodoscope and chamber inefficiencies and resolutions have been taken into account when generating the response of the apparatus. In addition to these signals, background hits determined from the data has been added. For the analysis of the deuterium data a more refined method has been used [22]. The simulated data were "digitised" and then passed through the full reconstruction chain to correct for imperfections in the off-line analysis. The mea-

Table 3. Systematic errors on the differential distributions of charged hadrons

Correction	Systematic error					
	$\frac{1}{N_\mu}\frac{dN}{dz}$		$\frac{1}{N_\mu}\frac{dN}{dp_t^2}$		$\langle p_t^2 \rangle$	
	p	d	p	d	p	d
Apparatus losses	4%	4%	4%	4%	–	–
Signal background	5%	3%	5%	3%	–	–
Hadronic reinteraction	5%	5%	5%	6%	3%	4%
Electron background	3%		5%		2%	
Track selection	7%	3%	7%	3%	5%	3%
Radiative corrections	2%	2%	2%	2%	2%	2%
Momentum measurement of μ, μ', h	3%	3%	5%	5%	2%	2%
Total systematic error	11%	8%	13%	10%	7%	6%

sured and simulated (accepted as well as generated) data of all SPS periods have been merged before performing the acceptance correction, in which the relative weights in the Monte Carlo data sets have been adjusted according to the number of scattered muons for each SPS period.

In Table 3 we show all the individual contributions to the total systematic error, which were considered to be relevant, for the normalised differential distributions $\frac{1}{N_\mu}\frac{dN}{dz}$, $\frac{1}{N_\mu}\frac{dN}{dp_t^2}$ and for $\langle p_t^2 \rangle$, separately for the hydrogen and deuterium analyses. These quantities do not depend on the absolute flux normalisation. The smaller errors for the latter analysis reflect a better understanding and simulation of the apparatus; a detailed discussion can be found in [17, 23]. All contributions have been added in quadrature as they are essentially uncorrelated. The final systematic errors are almost independent of the kinematics and are also given in Table 3. For the mean transverse momentum $\langle p_t^2 \rangle$ the systematic error is significantly smaller as contributions affecting the normalisation cancel. Neglecting normalisation uncertainties, the remaining systematic error amounts to about 60% of the quoted total systematic error. The final systematic errors have been checked by making comparisons between the different data sets in all variables.

4 Results

4.1 Scaled energy distributions

The normalised differential scaled energy distributions $\frac{1}{N_\mu}\cdot\frac{dN}{dz}$ have been determined separately for positive and negative hadrons as well as for all charged hadrons in small bins of x and Q^2 or W and Q^2. The bins are defined in Table 7 in the Appendix. The corresponding cross sections together with the mean values of the event variables are also presented in the Appendix (Tables 9–14).

Figure 1 shows the x and Q^2 dependence of the differential scaled energy distributions for all charged hadrons from both targets. Both data sets agree well within the statistical and systematic errors. This is expected within the QPM. Due to isospin invariance, the charge multiplicities of pions from scattering from protons and deuterons are expected to be equal. However, because of the presence of kaons and protons in the hadronic final state small differences are expected. Using the Lund fragmentation model [20] one can show that the expected differences should be smaller then 0.5% for $z<0.4$ and smaller than 2% for $z>0.4$. Such small differences are well below the accuracy of the data. The x- and Q^2-dependence present in the data is more clearly evident from the linear fits in $\ln Q^2$ to the data (see dotted lines in Fig. 1). The behaviour of the data has already been discussed in detail in previous EMC publications [24–26] using a subset of this data. Especially in [25] evidence for QCD scaling violations in the hadronic final state at fixed centre of mass energy W^2 has been presented. In particular it has been shown that the logarithmic slopes $\frac{d(1/N\cdot dN/dz)}{d\cdot \ln Q^2}$ as function of z show the pattern typical for QCD scaling violations.

The scaled energy distributions were compared with different versions of the Lund fragmentation model [18–20], which have been available during the data analysis. For this comparison we have merged the proton and deuteron data to form one high statistics data set (see Table 15 in the Appendix). Figure 2 shows the comparison of the merged data set with the following versions of the Lund models:

Model 1: Lund 4.3 (LEPTO 4.3, JETSET 4.3) – string model with soft gluon radiation;
Model 2: Lund 6.3 (LEPTO 5.2, JETSET 6.3) – string model with exact first order QCD calculation;
Model 3: Lund 6.3 (LEPTO 5.2, JETSET 6.3) – parton shower model.

The Lund 6.3 *matrix element* and the *parton shower* version (model 2 and 3) with their standard parameters describe the pattern of the data well in the whole kinematic range. The decreasing multiplicity for increasing Q^2 at high z is reasonably simulated by the inclusion of QCD processes. The older Lund version 4.3 (model 1) also describes qualitatively the kinematic dependences of the data.

4.2 Transverse momentum distributions

In this Sect. we present the p_t^2 dependence of the cross section for all charged particles. Because extensive studies [23] have not shown any significant difference between the proton and deuterium data, both data sets have been merged. The high statistics of the resulting data set allow studies of the cross sections up to high values of p_t^2 in different kinematical regions.

In Fig. 3 we show the inclusive p_t^2 distributions in z and W^2 bins. The corresponding cross sections are

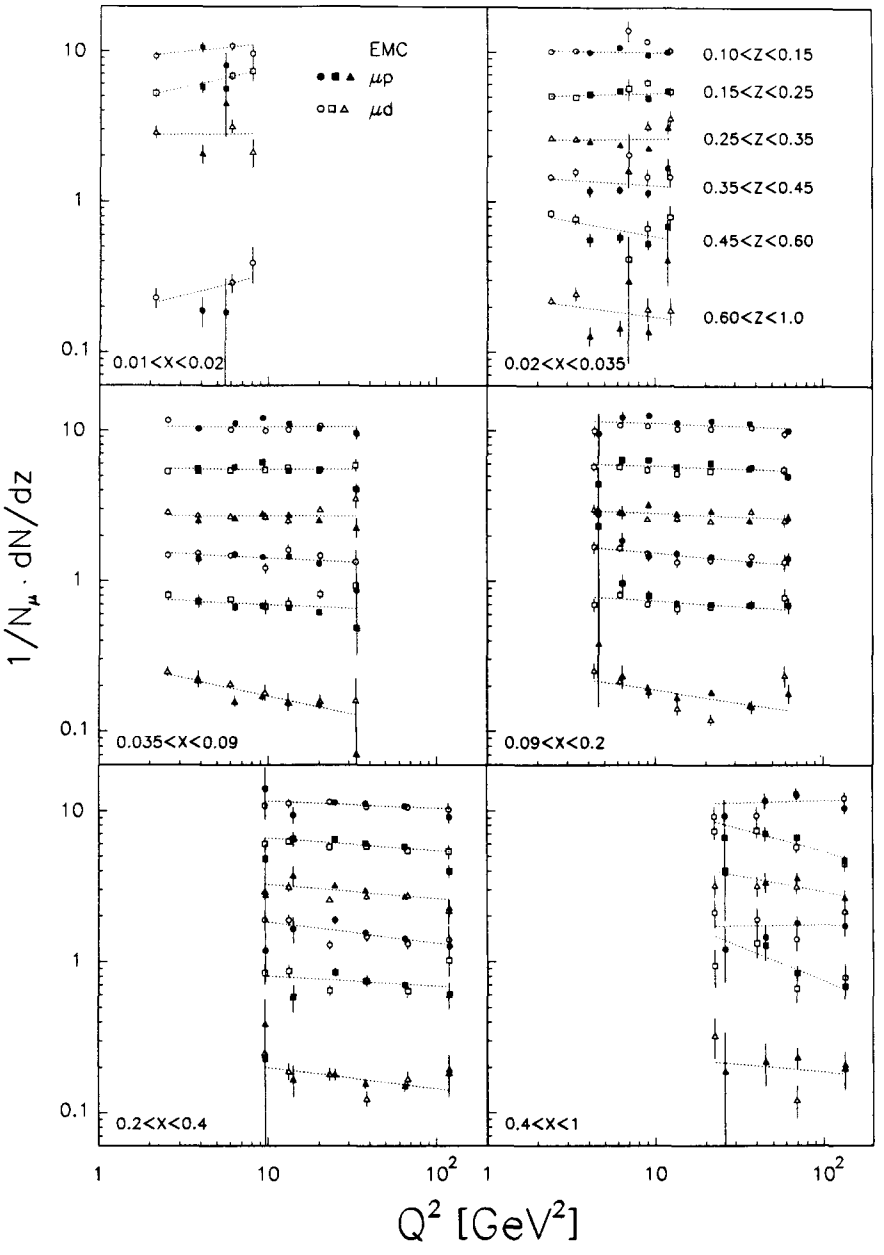

Fig. 1. Comparison of normalised differential scaled energy distributions for charged hadrons in bins of x, Q^2 and z. The dotted lines represent linear fits in $\ln Q^2$ inspired by QCD. The errors shown are statistical only

given in Tables 16a, b in the Appendix. At large values of p_t^2 a tail is observed, which clearly increases with W^2, as expected from QCD. The dotted lines are fits to the data using the ansatz $\frac{1}{N_\mu} \cdot \frac{dN_h}{dp_t^2} \propto 1/(m^2+p_t^2)^\alpha$, inspired by a propagator form. The mass term m obtained from the fits is in the range 0.6–1.6 GeV (excluding the very low z and W^2 bin), the power α is in the range 1.4–2.6, with a central value close to two. Thus the fall off of the measured cross section at large p_t^2 ($p_t^2 \gg m^2$) indicates the power law behaviour $\propto 1/p_t^4$, as expected from QCD.

Further, the measured mean squared transverse momentum $\langle p_t^2 \rangle$ for charged hadrons was analysed. Figure 4 shows the W^2 dependence of $\langle p_t^2 \rangle$ in z and Q^2 bins (Table 17). A linear increase of $\langle p_t^2 \rangle$ with $\ln W^2$ is seen for all z, Q^2 bins, and this is more pronounced in the high z region. The lines represent linear fits in $\ln W^2$ to the data.

To investigate a possible Q^2 dependence, such as that observed for the z distributions at fixed W^2 [25], we plot in Fig. 5 the fitted $\langle p_t^2 \rangle$ in each z bins for a central W^2 value of 200 GeV^2. The data for $Q^2 > 5$ GeV^2 show no Q^2 dependence. Only for the lowest Q^2 bin (2 GeV^2 $< Q^2 < 5$ GeV^2) the average p_t^2 is slightly smaller, which is presumably due to the contribution of elastic and quasi-elastic events. Because $x \approx (W^2/Q^2+1)^{-1}$, this implies no significant x dependence, except for very small x. This confirms, with increased precision, the conclusions of earlier EMC experiments [27, 28] that W^2 and z are the relevant variables for the p_t^2 behaviour.

In Fig. 6 the W^2 dependence of $\langle p_t^2 \rangle$ (see also Table 18) are compared to those from other experiments. Here the high precision of our data can be seen. They

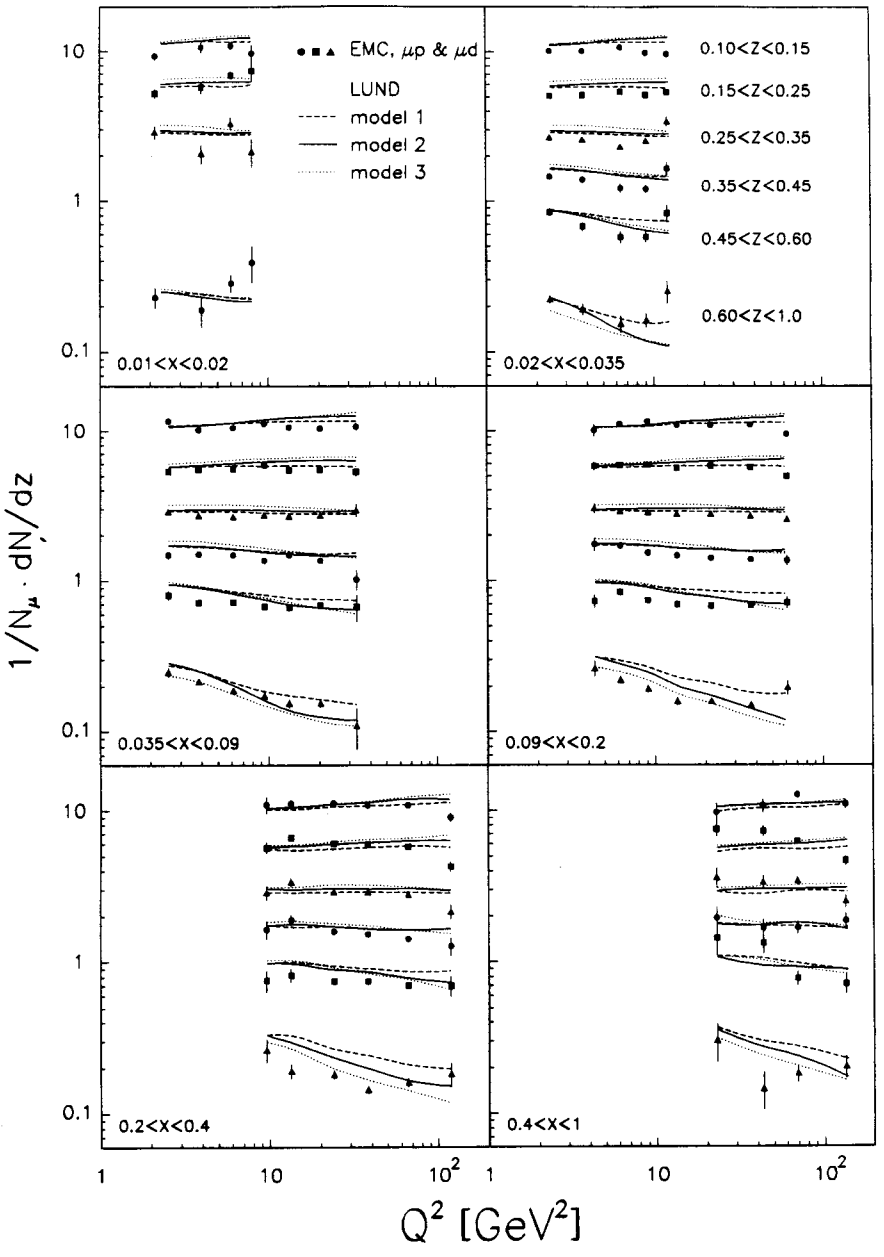

Fig. 2. Comparison of normalised differential scaled energy distributions for charged hadrons of the merged μp- and μd-data with different versions of the Lund fragmentation model [18, 20]. The errors shown are statistical only. The relative systematic error is 10%

agree well with the results of a νNe-scattering experiment a low W^2 range [29] and with the previous measurement of this experiment [27] apart from a slight discrepancy in the lowest z bin.

The $\langle p_t^2 \rangle$ dependence on z^2 for different W^2 bins is shown in Fig. 7. At small z^2 the expected rapid rise of $\langle p_t^2 \rangle$ with z^2 (seagull effect) is observed. This is more pronounced for the high W^2 bins. For $z > 0.4$, the increase is much smaller for the low W^2 bins; for the high W^2 bins $\langle p_t^2 \rangle$ reaches a plateau or even shows a falling trend.

Figure 8 compares $\langle p_t^2 \rangle$ as a function of W^2 with the different Lund models specified in Sect. 4.1. The default parameters have been used, of which the most important for $\langle p_t^2 \rangle$ are: $k_t = 0.44$ GeV, $\sigma_q = 0.4$ GeV, $\Lambda = 0.4$ GeV and the cutoff parameter (for model 3 only) $t_{\min} = 1$ GeV.

The parton shower model (model 3), which fits e^+e^- data well [32], fails to describe the size of $\langle p_t^2 \rangle$ as well as the dependence on W^2. This is due to an underestimation of the cross section at large p_t^2 [23]. Simple retuning of the model parameters does not change the p_t^2 behaviour sufficiently in order to describe the data [33]. The matrix element version of the model (model 2) describes the shape of the W^2 dependence. However, it underestimates $\langle p_t^2 \rangle$ significantly for large z ($z > 0.4$). This discrepancy cannot be cured by increasing the intrinsic k_t, because this would cause a disagreement with backward produced hadrons as shown earlier by the EMC [28]. Only the older version Lund 4.3 (model 1), which accounts for soft gluon radiation processes, reasonably describes the data, except for a small underestimation on $\langle p_t^2 \rangle$ in the highest z range.

The same behaviour of the models is demonstrated

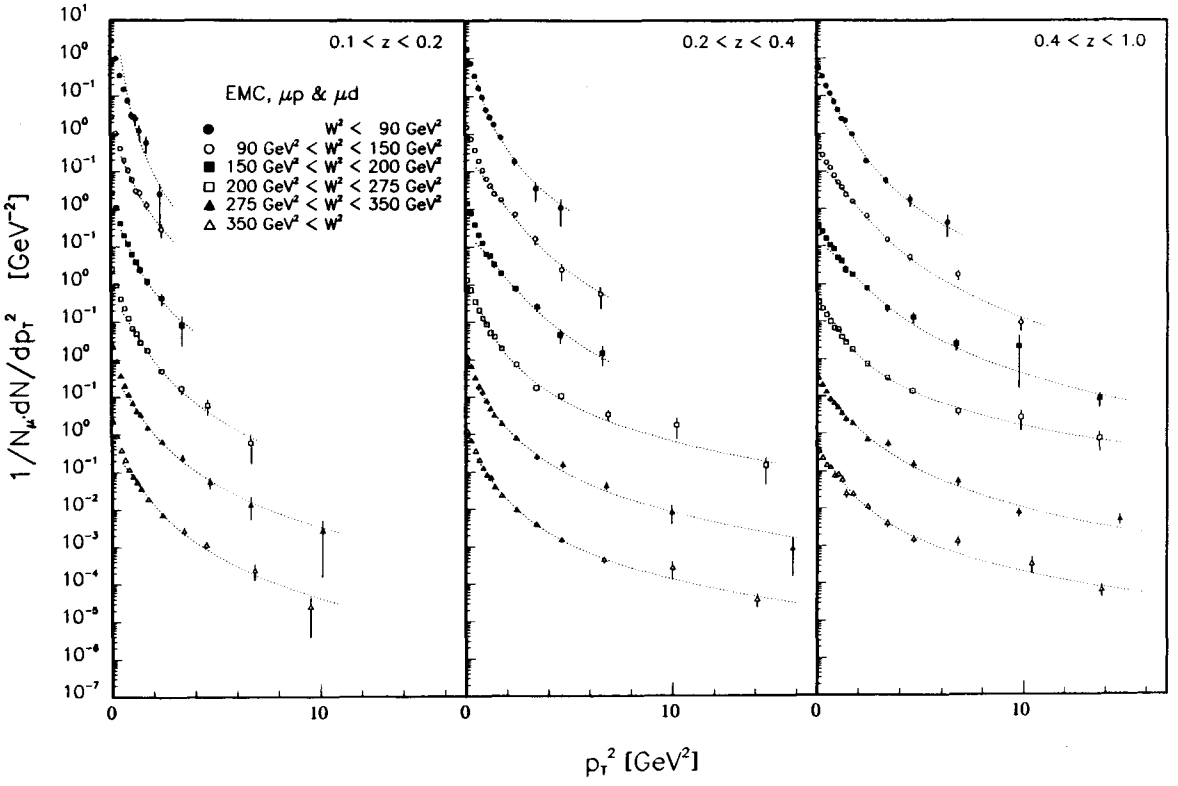

Fig. 3. Normalised differential p_t^2 distributions for charged hadrons of the merged μp- and μd-data in different W^2 and z bins. The dotted lines represent fits using the ansatz $\frac{1}{N_\mu}\cdot\frac{dN_h}{dp_t^2}\propto 1/(m^2+p_t^2)^a$ inspired by a propagator form. The errors shown are statistical only

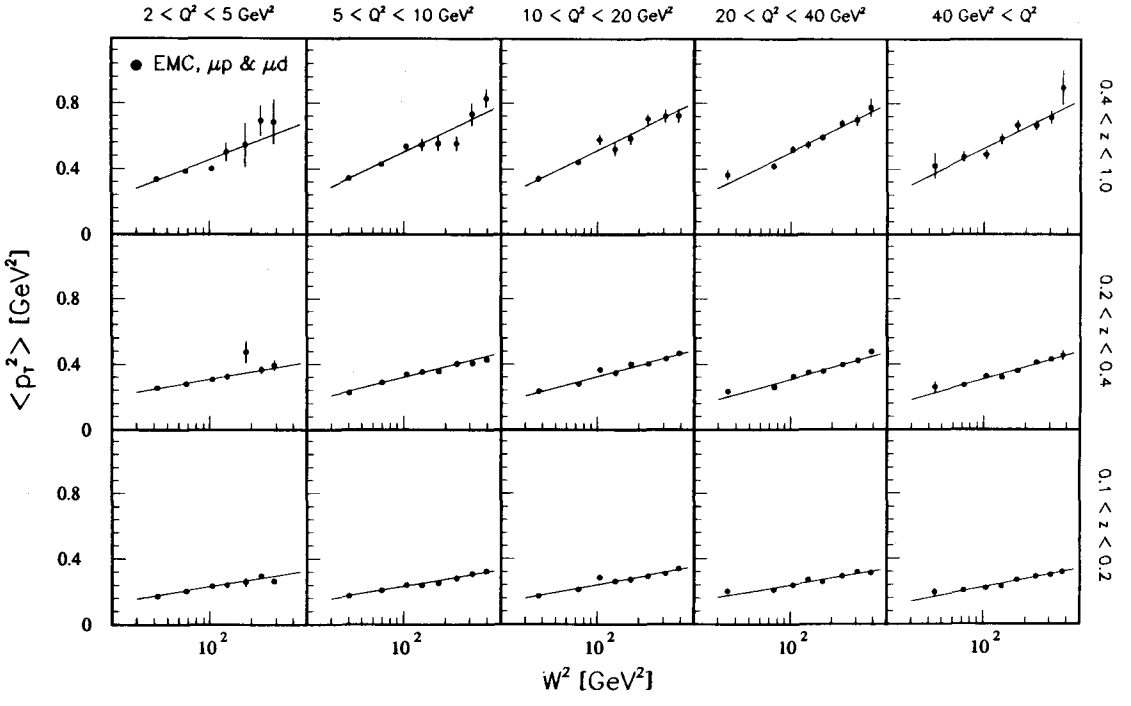

Fig. 4. W^2 dependence of $\langle p_t^2\rangle$ for charged hadrons in bins of Q^2 and z. The solid lines represent linear fits in $\ln W^2$. The errors shown are statistical only

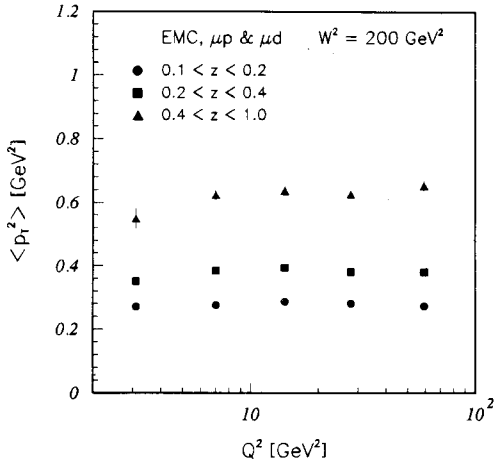

Fig. 5. $\langle p_t^2 \rangle$ of charged hadrons for fixed W^2 as a function of Q^2 in different z bins. The errors shown are statistical only

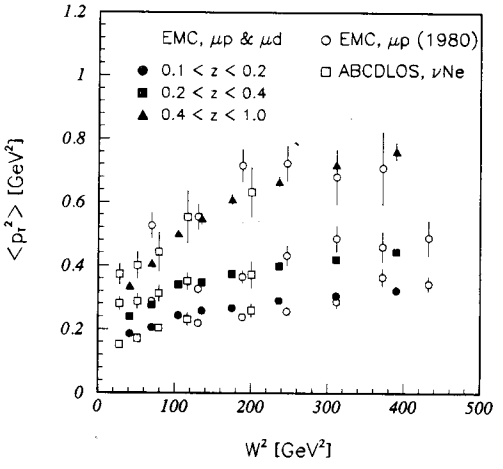

Fig. 6. Comparison of $\langle p_t^2 \rangle$ of charged hadrons as a function of W^2 with BEBC data of the collaboration ABCDLOS [29] and a previous EMC analysis [27]. The three z ranges for the data shown are the same for the three analyses. The errors shown are statistical only

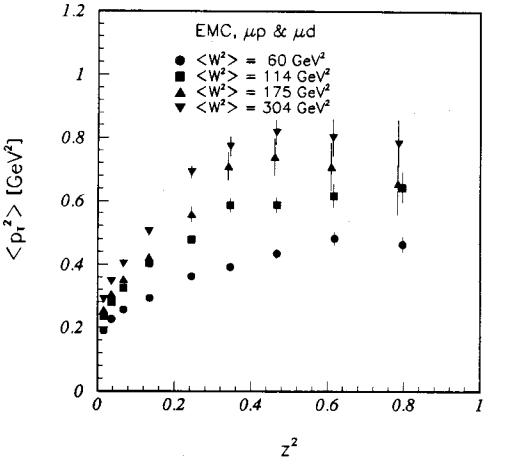

Fig. 7. z^2 dependence of $\langle p_t^2 \rangle$ (seagull effect) for charged hadrons in different W^2 bins. The errors are statistical only

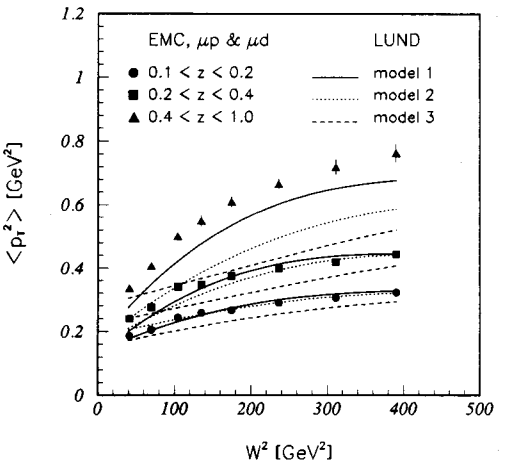

Fig. 8. Comparison of the W^2 and z dependence of $\langle p_t^2 \rangle$ of charged hadrons with different versions of the Lund fragmentation model [18, 20]. The errors shown are statistical only

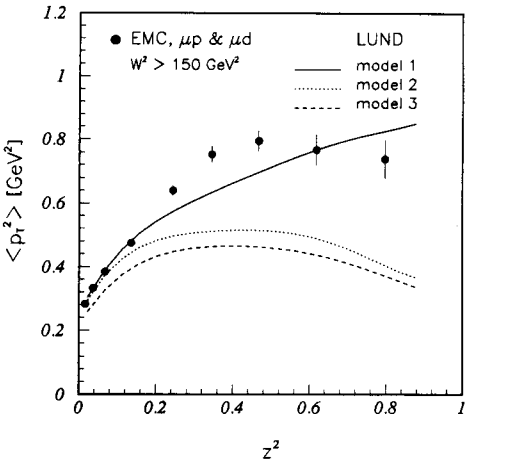

Fig. 9. Comparison of the z^2 dependence of $\langle p_t^2 \rangle$ of charged hadrons with different versions of the Lund fragmentation model [18, 20]. The errors shown are statistical only

in Fig. 9, where $\langle p_t^2 \rangle$ of hadrons produced at $W^2 > 150\,\mathrm{GeV}^2$ is plotted versus z^2. Model 1 shows again the best description, but the trend of the data to reach a plateau or eventually decrease at high z^2 is not reproduced.

Summarizing our comparisons to Monte Carlo models it can be said, that only the older Lund 4.3 model (model 1), which includes contributions due to soft gluon radiation, is able to describe both the z and p_t^2 behaviour of the data.

4.3 Charge multiplicity ratios

In this Sect. we compare ratios of charge multiplicities for μ-scattering from protons, deuterons and neutrons. The derivation of the charged hadron production rates from neutrons was performed using (2). Figure 10 shows the ratio of the integrated charge multiplicities for muon scattering from protons, deuterons and neutrons versus

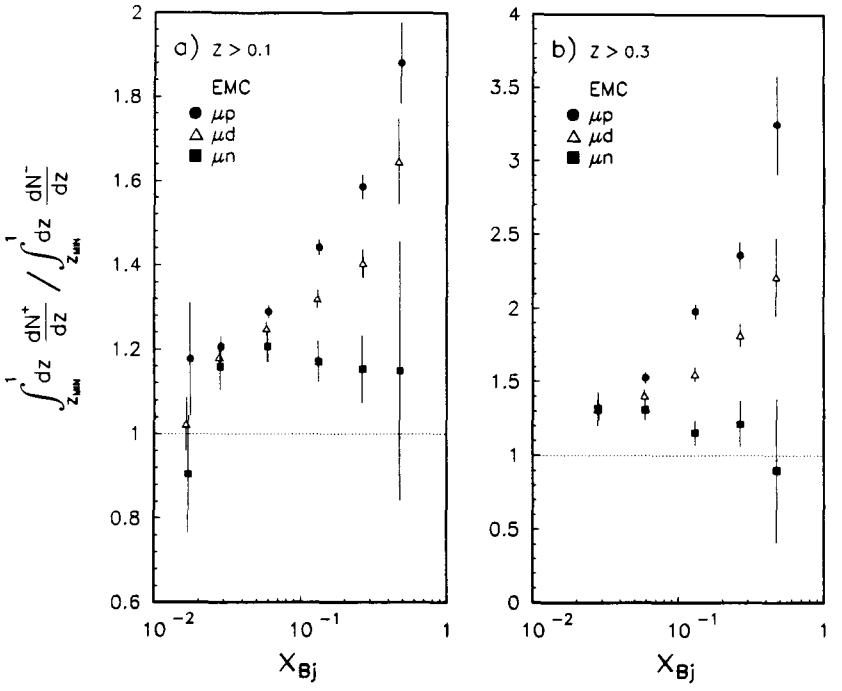

Fig. 10a, b. Ratio of the integrated charge multiplicities as a function of x for two different z ranges. The errors shown are statistical only

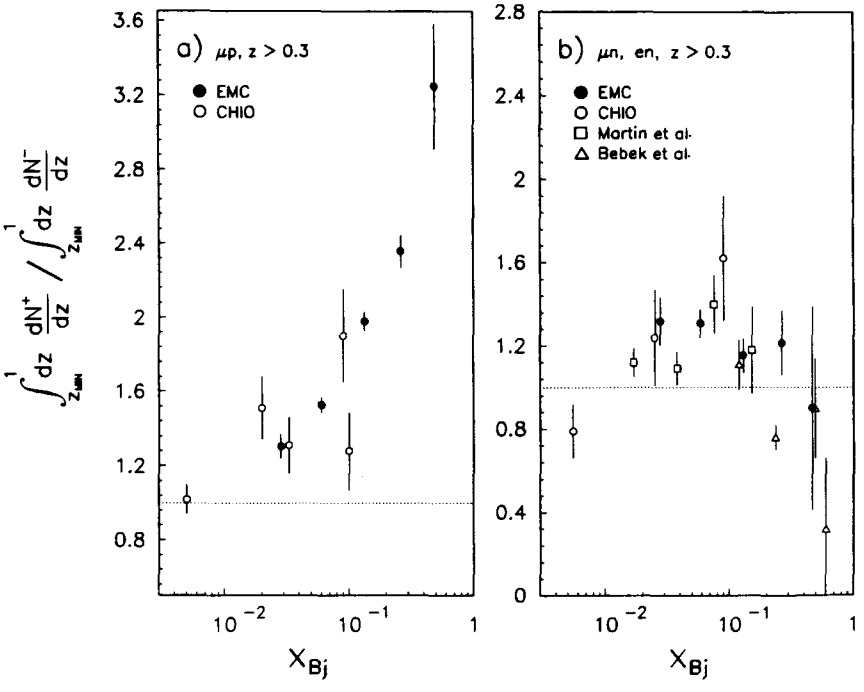

Fig. 11a, b. Ratio of integrated charge multiplicities as a function of x; **a** Comparison of the ratio from the μp-data to [35]; **b** Comparison of the ratio from the μn-data to [35, 36]; The errors shown are statistical only

x in two different regions of z, from 0.1 to 1 and from 0.3 to 1. The data have been integrated over the whole Q^2 range, as, for the ratios, no significant dependence on Q^2 was seen in our data. Generally, the observed x dependence is stronger for the higher z range, as with increasing z the probability ratios are closer to unity for p, d and n. Here fragmentation effects and resonance decays dominate. The x dependence of the charge multiplicity ratios in small bins of z can be found in Table 19 in the Appendix.

The observed x dependence of the charge multiplicity ratios can be interpreted as follows. At small x, the ratios for muon scattering from all these targets approach each other close to unity due to the dominant contribution of the sea quarks to the cross section. For increasing x we see, when scattering from the proton, the expected strong increase of the excess of positive particles due to the dominance of the positive u quarks at high x. This effect is still seen for the isoscalar deuteron, as the virtual photon couples preferentially to the positive u quark. For the neutron we observe, for both z ranges, that the charge multiplicity ratio is significantly above unity for a wide range of the x region covered by our data.

A neutral electromagnetic current probing a neutral target shows an excess of positive charged hadrons in the forward scattering hemisphere over a wide kinematic range. This proves a charge composition of the neutron, where the magnitude of the charge of the positive constituents must be greater than that of the negative, also implying more than two charged constituents. This was also observed at a significant level in a previous publication [34]. In addition, contrary to the proton and deuteron data, the charge multiplicity ratio for the neutron shows a slight decrease with x. This confirm independently the behaviour of the quark distribution functions inferred from the structure functions measurements; at high x the $d_v(x)$ distribution in the neutron predominates over the $u_v(x)$. A cross over to negative values of the ratio is expected for x between 0.5 and 0.6.

The systematic error on the measured charge multiplicity ratio for the neutron is estimated to be 3% for low x rising to 12% for the highest x data point. It is dominated by the uncertainty of the different acceptances for positive and negative hadrons in the EMC forward spectrometer [17].

In the low x region a comparison can be made with a previous experiment [35] in a similar energy range. The data agree well in the overlap region for both, μp- and μn-scattering (see Fig. 11a, b).

4.4 Determination of $d_v(x)/u_v(x)$

Taking the difference of the normalised scaled energy distribution (1) for positive and negative hadrons the contribution of the sea quarks cancels exactly. Using charge conjugation symmetry $[D^h_{q_i}(z, Q^2)=D^{\bar{h}}_{\bar{q}_i}(Q^2)]$ and the definition of valence quark distributions $[q_v(x, Q^2) = q(x, Q^2)-q_s(x, Q^2)]$, the following equation can be derived

$$\frac{1}{N_\mu}\left(\frac{\mathrm{d}N^{h^+}}{\mathrm{d}z}-\frac{\mathrm{d}N^{h^-}}{\mathrm{d}z}\right)=\frac{x}{F_2}\cdot(e_u^2\,u_v(D_u^{h^+}-D_u^{h^-}) + e_d^2\,d_v(D_d^{h^+}-D_d^{h^-})), \tag{4}$$

where $\sum_{i=u,d,\ldots} e_i^2\,q_i$ has been replaced by the corresponding structure function F_2.

Considering only the production of pions in the hadronic final state, then using isospin invariance $[(D_u^{\pi^+}=D_{\bar{d}}^{\pi^-}), (D_u^{\pi^-}=D_{\bar{d}}^{\pi^+}), (u_v^p=d_v^n=:u_v), (d_v^p=u_v^n=:d_v)]$, (4) can be rewritten for muon scattering from protons and neutrons separately as follows:

$$\frac{1}{N_\mu^p}\left(\frac{\mathrm{d}N_p^{\pi^+}}{\mathrm{d}z}-\frac{\mathrm{d}N_p^{\pi^-}}{\mathrm{d}z}\right)\mathrm{d}z = \frac{x}{F_2^p}\cdot(e_u^2\,u_v-e_d^2\,d_v)\cdot(D_u^{\pi^+}-D_u^{\pi^-})\,\mathrm{d}z,$$

$$\frac{1}{N_\mu^n}\left(\frac{\mathrm{d}N_n^{\pi^+}}{\mathrm{d}z}-\frac{\mathrm{d}N_n^{\pi^-}}{\mathrm{d}z}\right)\mathrm{d}z = \frac{x}{F_2^n}\cdot(e_u^2\,d_v-e_d^2\,u_v)\cdot(D_u^{\pi^+}-D_u^{\pi^-})\,\mathrm{d}z. \tag{5}$$

To improve the accuracy of the experimental evaluation, the above equations can be integrated over a range in z. Taking the ratio of these integrated equations, the difference of the fragmentation functions cancels and one can directly solve for $d_v(x)/u_v(x)$ which, for fixed Q^2, is a function of x only

$$\frac{d_v(x)}{u_v(x)}=\frac{4\cdot\mathscr{R}^\pi(x)+1}{4+\mathscr{R}^\pi(x)}, \tag{6}$$

where $\mathscr{R}^\pi(x)$ is to be measured by the experiment

$$\mathscr{R}^\pi(x):=\frac{\frac{1}{N_\mu^n}\int_{z_1}^{z_2}\left(\frac{\mathrm{d}N_n^{\pi^+}}{\mathrm{d}z}(x)-\frac{\mathrm{d}N_n^{\pi^-}}{\mathrm{d}z}(x)\right)\mathrm{d}z}{\frac{1}{N_\mu^p}\int_{z_1}^{z_2}\left(\frac{\mathrm{d}N_p^{\pi^+}}{\mathrm{d}z}(x)-\frac{\mathrm{d}N_p^{\pi^-}}{\mathrm{d}z}(x)\right)\mathrm{d}z}\cdot\frac{F_2^n(x)}{F_2^p(x)}. \tag{7}$$

In this experiment the possibility to identify hadrons is limited. Therefore (6) has to be corrected for the presence of charged kaons and (anti-)protons in the hadronic final state, but as pions are the dominant particles, the correction is expected to be small. If one includes the fragmentation into charged kaons and (anti-)protons, the ratio takes the following form

$$\frac{d_v(x)}{u_v(x)}=\frac{4\cdot\mathscr{R}^h(x)+1-\Delta}{4+\mathscr{R}^h(x)(1-\Delta)}, \tag{8}$$

where $\mathscr{R}^h(x)$ denotes the same ratio as $\mathscr{R}^\pi(x)$ above, except that all hadrons are used now instead of only pions in case of $\mathscr{R}^\pi(x)$. Δ contains only the fragmentation functions, which in the QPM are independent of the scattering process thus independent of x:

$$\Delta=1-\frac{\int_{z_1}^{z_2}(D_d^{h^-}-D_d^{h^+})\,\mathrm{d}z}{\int_{z_1}^{z_2}(D_u^{h^+}-D_u^{h^-})\,\mathrm{d}z}. \tag{9}$$

Δ is limited to be between 0 and 1 and has been estimated with the recent fragmentation models by the Lund group [19, 20] to be 0.4 ± 0.1. For the experimental evaluation of (8), all quantities in $\mathscr{R}^h(x)$ containing hadron production rates from neutrons have to be expressed by production rates from deuterons using (2). Further, after integration over the whole range accessible in z, it becomes

$$\mathscr{R}^h(x):=\frac{\frac{1}{N_\mu^d}\int_{0.1}^{1}\left(\frac{\mathrm{d}N_d^{h^+}}{\mathrm{d}z}(x)-\frac{\mathrm{d}N_d^{h^-}}{\mathrm{d}z}(x)\right)\mathrm{d}z}{\frac{1}{N_\mu^p}\int_{0.1}^{1}\left(\frac{\mathrm{d}N_p^{h^+}}{\mathrm{d}z}(x)-\frac{\mathrm{d}N_p^{h^-}}{\mathrm{d}z}(x)\right)\mathrm{d}z}\cdot\left(1+\frac{F_2^n(x)}{F_2^p(x)}\right)-1. \tag{10}$$

Figure 12 shows the difference of the integrated charge multiplicities in the z range 0.1–1 for muon scattering from protons and deuterons in different bins of x. The main systematic uncertainties in the determination of $d_v(x)/u_v(x)$, which are discussed in more detail in [17], are the following:

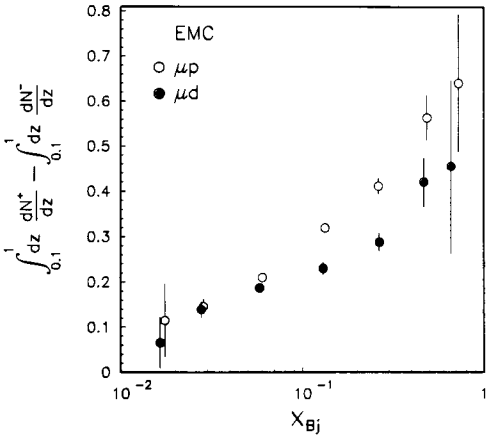

Fig. 12. Difference of integrated charge multiplicities from μp- and μd-scattering as a function of x. The errors shown are statistical only

- determination of Δ: The Lund model gives a satisfactory description of the scaled energy distributions and particle composition in deep inelastic lepton nucleon scattering [38] as well as for e^+e^- annihilation experiments [39]. As Δ contains only the process independent fragmentation functions, and is independent of x, this term can be estimated using this fragmentation model. Reasonable variations of the fragmentation functions, which respect both energy and momentum conservation lead to a change of Δ always smaller than 20%. This leads to a 1% uncertainty in $d_v(x)/u_v(x)$ at small x and 6% at high x.
- QCD effects: As the derivation of (8) is valid in the leading log approximation of QCD, only higher order effects may affect it. Detailed studies with the Lund model [20], containing QCD processes up to first order in α_s, allow to estimate the corrections to the data. They influence $d_v(x)/u_v(x)$ by at most -3% at $x=0.1$ and less than -1% at small and large x. This is confirmed by the parton shower version [20]. The correction is small since the main contribution coming from the fragmentation of hard gluons cancels exactly, because only differences of charge multiplicities are being used. The uncertainty is assumed to be half of the correction. Non perturbative QCD effects (higher twists) in the structure functions, as well as in the hadronic final state, have been shown to be negligible in the kinematic range of this experiment [26, 40]. This is also valid for the elastic or quasi-elastic production of resonances [41].
- Acceptance corrections: To keep the systematic uncertainties of the differences as small as possible, the charge multiplicities have been renormalised such that the sum of the positive and negative charge multiplicities for the proton and deuteron data agree with their average. These corrections are of the order of 5% and are mainly due to global normalisation shifts between the data sets. The uncertainty in the absolute normalisation cancels, as only the ratio of multiplicities is needed. The remaining uncertainties are due to the different acceptances of the spectrometer for positive and negative charged particles varying with x.

Table 4. Sources of systematic errors of $d_v(x)/u_v(x)$

Absolute systematic error of $d_v(x)/u_v(x)$		
Source of uncertainty	$x=0.03$	$x=0.5$
Charge multiplicity difference (acceptance correction + QCD processes)	0.025	0.065
Determination of Δ	0.01	0.02
$F_2^n(x)/F_2^p(x)$	0.03	0.04
Total systematic error	0.04	0.08

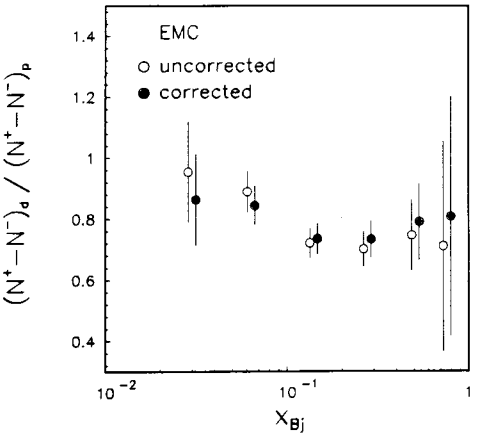

Fig. 13. Ratio of the differences of the integrated charge multiplicities from μp- and μd-scattering as a function of x. $N^{+(-)}$ denotes the integral $\frac{1}{N_\mu}\int_{0.1}^{1} dz \frac{dN}{dz}$ for positive and negative particles respectively. The ratio is shown before and after the corrections discussed in Sect. 4.4. The errors shown are statistical only

- structure functions: As the ratio of structure functions $F_2^n(x)/F_2^p(x)$ is needed, only the relative normalisation uncertainty contributes. For the ratio, the same linear parametrisation of the EMC data [7] is used as for the determination of the neutron rate (see Sect. 2). The uncertainty is assumed to be 5–10% depending on x.

Table 4 contains the systematic uncertainties for $d_v(x)/u_v(x)$ deduced from the above considerations. Figure 13 shows the ratio of the differences of deuterium to proton data, before and after the corrections discussed above. The changes are well within the statistical errors.

Figure 14a, and also Table 5, show the final result for $d_v(x)/u_v(x)$. The error bars of the data points represent the statistical errors, the systematic uncertainty is drawn at the bottom of the picture.

Figure 14b shows the data points, together with previous measurements of two neutrino scattering experiments [42, 43]. For the EMC and CDHS data statistical and systematic errors have been added in quadrature. For the BEBC data no systematic errors have been quoted, therefore the errors shown are purely statistical. It can be seen that the ratio decreases below 1/2 with increasing x. This measurement is in good agreement with the results of the neutrino experiments, obtained with a completely different method. For $x<0.1$ there is a ten-

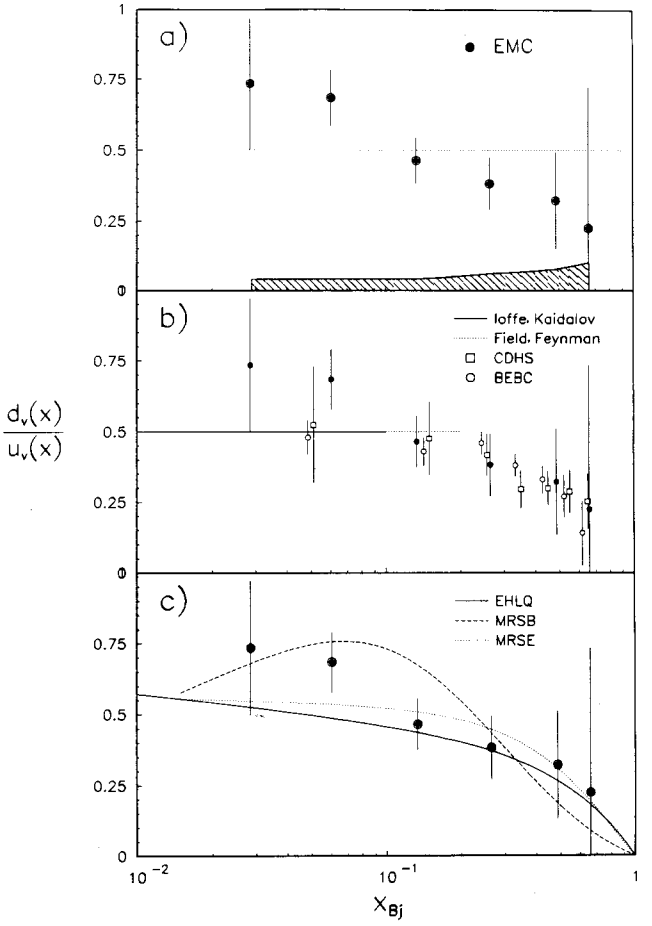

Fig. 14a–c. **a** Ratio of the valence distribution d_v/u_v as a function of x; the shaded area indicates the systematic error. The dotted line represents the expectation of the naive QPM of $\frac{1}{2}$. **b** Comparison with the ν-scattering experiments BEBC [42] and CDHS [43]. The lines represent two theoretical predictions using Regge arguments (solid line [44], dotted line [45]). For the EMC and CDHS data statistical and systematic errors are added in quadrature. For the BEBC data no systematic errors have been quoted. **c** Comparison with different parameterisations of the quark distribution functions. DFLM [46] is based on neutrino data only, whereas MRSB and MRSE [47] is derived with additional information taken from the deep inelastic muon nucleon scattering experiments BCDMS (dotted curve) and EMC (dashed curve)

Table 5. $d_v(x)/u_v(x)$ with errors and mean values of the variables x and Q^2

$\langle x\rangle$	$\langle Q^2\rangle$	$d_v(x)/u_v(x)$	σ_{stat}	σ_{sys}
0.028	6.5	0.74	0.23	0.04
0.059	9.2	0.68	0.10	0.04
0.132	18.9	0.47	0.08	0.04
0.265	37.5	0.38	0.09	0.06
0.476	62.5	0.32	0.17	0.08
0.660	90.6	0.24	0.50	0.10

dency of the EMC data to be higher than the data of the neutrino experiments.

There are no theoretical predictions about the functional behaviour of $d_v(x)/u_v(x)$. For small x there are two theoretical considerations, based on Regge arguments, which expect the ratio to be 1/2, for x less than 0.2 [45] respectively. These are excluded already by the data at $x>0.1$. To fulfil the fundamental sum rules $\int_0^1 u_v(x)\,dx=2$, $\int_0^1 d_v(x)\,dx=1$, the ratio has to be greater than 1/2 somewhere in the low x region, as it is less than 1/2 for high x. Such behaviour is indicated by the EMC data. The height of the necessary increase of $d_v(x)/u_v(x)$ above 1/2 is dependent on the absolute valence quark distributions. Therefore Fig. 14c compares the data with selected quark distribution parameterisations, which fulfil the above sum rules. The solid curve shows the parameterisation by DFLM [46], based on neutrino data only. For the dashed and dotted curves by MRS [47], the neutrino data are used only to fix the sum of the valence distributions $d_v(x)+u_v(x)$. The remaining information needed was taken from the deep inelastic muon nucleon scattering experiments of the BCDMS (dotted curve) and the EMC (dashed curve). The first parameterisation is similar to the parameterisation by DFLM while the second parameterisation shows a significant increase above 1/2 at lower x, still fulfilling the sum rules. This analysis cannot discriminate between the parameterisations.

Finally, the ratio $d_v(x)/u_v(x)$ characterises the structure of the nucleon with respect to the dynamical distribution of the valence quarks. The good agreement between the results coming from deep inelastic μ-nucleon scattering and the results from neutrino scattering shows that, in addition to the absolute structure function measurements, the charged and neutral currents are probing the same substructure of the nucleon.

4.5 Determination of the sum rule by Gronau et al. and determination of the quark charges

The sum rule derived by Gronau, Ravndal and Zarmi [1] correlates the number of valence quarks inside the nucleon with their electric charges. The sum rule can be obtained by integrating (5) over the entire range in x from 0 to 1 in order to replace the quark distribution function by the number of valence quarks. For the ratio, the fragmentation functions cancel, giving

$$\mathscr{R}^{\pi}_{\mathrm{Gr}}=\frac{(e_u^2\cdot 1-e_d^2\cdot 2)}{(e_u^2\cdot 2-e_d^2\cdot 1)}=\frac{2}{7}, \tag{11}$$

where $\mathscr{R}^{\pi}_{\mathrm{Gr}}$ is the quantity to be measured by the experiment

$$\mathscr{R}_{\pi\mathrm{Gr}}:=\frac{\int_0^1\left[\frac{F_2^n(x)}{x}\frac{1}{N_\mu^n}\int_{z_1}^{z_2}\left(\frac{dN_n^{\pi^+}}{dz}(x)-\frac{dN_n^{\pi^-}}{dz}(x)\right)dz\right]dx}{\int_0^1\left[\frac{F_2^p(x)}{x}\frac{1}{N_\mu^p}\int_{z_1}^{z_2}\left(\frac{dN_p^{\pi^+}}{dz}(x)-\frac{dN_p^{\pi^-}}{dz}(x)\right)dz\right]dx}. \tag{12}$$

Apart from the assumed number of one d and two u valence quarks inside the proton and their electric charges, (11) and (12) contain only directly measurable

quantities; namely, the absolute structure functions F_2 and differences of charge multiplicities. As for the determination of $d_v(x)/u_v(x)$, we have to correct this relation for the presence of kaons and (anti-)protons in the hadronic final state. Again the correction term Δ (9) appears

$$\mathscr{R}^h_{\mathrm{Gr}} = \frac{2}{7} \cdot \left(\frac{1+\Delta}{1+\frac{\Delta}{7}} \right). \tag{13}$$

Rewriting the sum rule in the original form and using the hadron production rates from protons and deuterons for $\mathscr{R}^h_{\mathrm{Gr}}$ one can write the Gronau et al. sum rule as follows

$$\mathscr{R}^{\pi}_{\mathrm{Gr}} = \frac{(e_u^2 \cdot 1 - e_d^2 \cdot 2)}{(e_u^2 \cdot 2 - e_d^2 \cdot 1)} = \frac{2}{7} = \mathscr{R}^h_{\mathrm{Gr}} \cdot \left(\frac{1+\frac{\Delta}{7}}{1+\Delta} \right), \tag{14}$$

where the measurable quantity $\mathscr{R}^h_{\mathrm{Gr}}$ is

$$\mathscr{R}^h_{\mathrm{Gr}} := \frac{\int_0^1 \left[\frac{F_2^d(x)}{x} \frac{1}{N_\mu^d} \int_{0.1}^1 \left(\frac{\mathrm{d}N_d^{h^+}}{\mathrm{d}z}(x) - \frac{\mathrm{d}N_d^{h^-}}{\mathrm{d}z}(x) \right) \mathrm{d}z \right] \mathrm{d}x}{\int_0^1 \left[\frac{F_2^p(x)}{x} \frac{1}{N_\mu^p} \int_{0.1}^1 \left(\frac{\mathrm{d}N_p^{h^+}}{\mathrm{d}z}(x) - \frac{\mathrm{d}N_p^{h^-}}{\mathrm{d}z}(x) \right) \mathrm{d}z \right] \mathrm{d}x} - 1. \tag{15}$$

For this measurement we used the charge multiplicity differences as shown in Fig. 12. For the absolute structure functions $F_2^{n,p}$ we have used fits to the EMC proton and deuteron data [12, 48]. The integral contains a factor F_2/x diverging proportionally to the rise of the sea in the nucleon. However, this term is multiplied by the charge multiplicity difference $\left(\frac{\mathrm{d}N^{h^+}}{\mathrm{d}z}(x) - \frac{\mathrm{d}N^{h^-}}{\mathrm{d}z}(x) \right)$, which approaches zero as the contribution of the symmetric sea to the cross section increases. So we expect the integral to converge at small x.

Figure 15a shows the two integrals used for the determination of $\mathscr{R}^h_{\mathrm{Gr}}$ as a function of the lower limit of the integral $x_{\min}$. The data indicate a converging behaviour, but clearly, the limit is not reached at the smallest values of $x_{\min}$. As both integrals follows the same functional behaviour (see definition of $\mathscr{R}^h_{\mathrm{Gr}}$, (15)), the ratio is expected to converge faster. This is shown in Fig. 15b where only a small variation of the ratio over the whole range in $x_{\min}$ is seen. Therefore we use the value $\mathscr{R}^h_{\mathrm{Gr}} = 1.41 \pm 0.06$ at $x_{\min} = 0.02$ for the determination of the sum rule. The lower limit of x has been chosen so as to minimize the final experimental error for the sum rule.

The sources of systematic uncertainties are summarised in Table 6. The main uncertainty is due to the structure function measurements, where only the relative normalisation uncertainty between proton and deuteron data [49] contributes significantly. Changing the absolute normalisation of the structure functions to the normalisation obtained by BCDMS [50] gives only a minor contribution as can be seen in the Table. Another significant contribution to the systematic error is due to the determination of the charge multiplicity differences and the correction Δ, as already discussed in the previous section. In addition, the absolute normalisation uncertainty for the charge multiplicities has to be included. The uncertainty due to the unmeasured part of the integrals between $x = 0$–0.02 was estimated using many different parameterisations of the valence distributions [51]. It was found that these parts influence the result of the sum rule in average by 2%. As a further consistency check, the lower boundary of the integral in z in formula 15 has been set to 0.15 and 0.2 leading to changes of -10% and $+5\%$ respectively, which are consistent with the statistical errors.

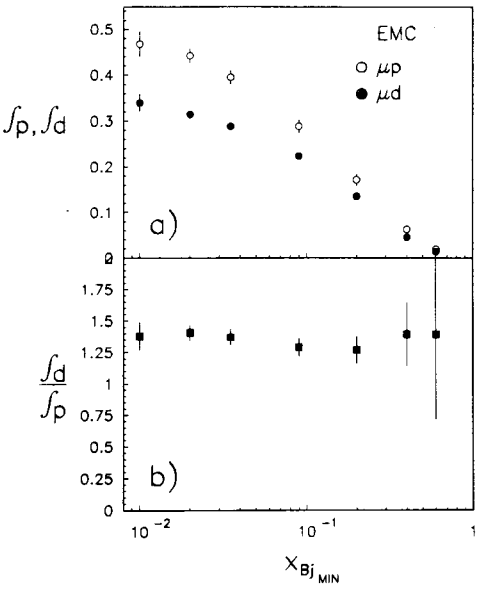

Fig. 15a, b. Integrals for the determination of the Gronau et al. sum rule as a function of the lower x bound; **a** $\int_p$ denotes the integral in the nominator and $\int_d$ in the denominator of (15), both integrals are shown separately; **b** shows the ratio of both integrals. The errors shown are statistical only

Table 6. Sources of systematic errors of the Gronau et al. sum rule

Relative systematic errors of the Gronau et al. sum rule	
Uncertainty	Error
Charge multiplicity difference:	
absolute normalisation (7%)	2%
acceptance correction + QCD processes	6%
Structure functions:	
relative normalisation of F_2^p versus F_2^d (3%)	14%
behaviour in x compared to BCDMS	1%
Determination of Δ	6%
Contribution to the integral from unmeasured region ($x = 0$–0.02)	2%
Total systematic error	17%

Finally, the value of the right hand side of the sum rule (14) is determined to be

$$\frac{(e_u^2 \cdot 1 - e_d^2 \cdot 2)}{(e_u^2 \cdot 2 - e_d^2 \cdot 1)} = 0.31 \pm 0.06_{\mathrm{stat}} \pm 0.05_{\mathrm{sys}}.$$

This is in good agreement with the expected value of 2/7 ($\cong 0.286$). An earlier measurement [37] yielded 0.24 ± 0.28, where the error is statistical only. The present analysis is the first significant test of this sum rule.

Assuming that there are one d and two u valence

quarks in the proton, one can directly extract the absolute ratio of quark charges

$$\frac{|e_d|}{|e_u|} = 0.44 \pm 0.10_{\text{stat}} \pm 0.08_{\text{sys}}.$$

The result shows that the absolute charge of the d quark is lower than the u quark charge and is in good agreement with the QPM expectation of 1/2.

Finally, the absolute charges of the u and d quark separately can be determined using the ratio of the structure functions $\frac{F_2^{\mu N}}{F_2^{\nu N}} = \frac{e_u^2 + e_d^2}{2} = 0.289 \pm 0.006_{\text{stat}} \pm 0.015_{\text{sys}}$ measured in deep inelastic muon nucleon and neutrino nucleon scattering [7]

$$|e_u| = 0.66 \pm 0.03_{\text{stat}} \pm 0.05_{\text{sys}},$$

$$|e_d| = 0.37 \pm 0.05_{\text{stat}} \pm 0.05_{\text{sys}}.$$

The result confirms very well the QPM expectations.

5 Summary

Precise charged hadron multiplicity spectra have been presented as a function of z in fine (Q^2, x_{Bj}) and (Q^2, W) bins for muon scattering from protons and deuterons. The data show the pattern of scaling violation and factorisation breaking expected from QCD. The corresponding p_t^2 spectra show a tail at large p_t^2, more pronounced at high z and W^2, which falls $\propto \frac{1}{p_t^4}$ as expected from QCD. The average squared transverse momentum can be described at fixed z by a linear dependence on $\log W^2$ only. No significant Q^2 dependence is observed withing the small statistical and systematic errors of our data for Q_2 bigger than 5 GeV^2.

The matrix element and parton shower versions of the Lund 6.3 model fail to reproduce the shape of the p_t^2 spectra, however, they describe well the pattern of z spectra. The older Lund 4.3 matrix element model, which includes contribution due to soft gluon radiation, describes resonably well the z and p_t^2 behaviour of the data.

The charge multiplicity ratios have been deduced for muon scattering from protons, deuterons and neutrons. They show stronger dependences for higher z ranges, as expected if the fast hadrons contain the struck quark. For protons a strong rise with x_{Bj} is observed. This is due to the excess of u quarks in the proton at large x_{Bj}. For deuterons the increase is less pronounced. The charge multiplicity ratio for neutrons is positive and decreases slightly with x_{Bj}. This proves, in a model independent way, that the neutron has more than 2 charged constituents and that the positive constituents carry a bigger charge than the negative. The tendency of the ratio to decrease with increasing x_{Bj} can be understood by the dominance of the d quark in the neutron at large x_{Bj}.

A novel method has been presented to extract, for the first time in charged lepton scattering, the ratio of the valence quark distributions $d_v(x)/u_v(x)$ from the measured charge multiplicity differences. The result agrees with previous neutrino measurements obtained by a different method and also extends the measurements to smaller x_{Bj}. In this region the ratio $d_v(x)/u_v(x)$ is bigger than expected from Regge considerations.

Finally, the Gronau et al. sum rule has been tested; the measured sum being $0.31 \pm 0.06 \pm 0.05$, compared to the theoretical expectation of $2/7 = 0.286$. This is the first significant test of this sum rule. From the measured sum, the absolute ratio of the d to u quark charges has been inferred to be $|e_d|/|e_u| = 0.44 \pm 0.10_{\text{stat}} \pm 0.08_{\text{sys}}$. Together with results of the average squared quark charge extracted from the neutrino and charged lepton structure function measurement, the absolute electric charges of the u and d quark are determined to be $|e_u| = 0.66 \pm 0.03 \pm 0.05$ and $|e_d| = 0.37 \pm 0.05 \pm 0.05$, respectively.

We wish to thank all people who have contributed to the construction and maintenance of our apparatus and to the analysis of this data. Especially, we want to thank those collegues of the early EMC, not signing this late analysis, who provided us with the hydrogen data and valuable comments.

Appendix

The appendix contains the Tables for the normalised differential scaled energy distributions $\frac{1}{N_\mu} \cdot \frac{dN}{dz}$ for positive and negative hadrons as well as for all charged hadrons in small bins of x and Q^2 (Tables 9–11) or W and Q^2 (Table 12–14) and for the merged proton and deuteron data set (Table 15). Tables 16a, b contain the inclusive p_t^2 distributions in z and W^2 bins. The W^2 dependence of the mean transverse momentum $\langle p_t^2 \rangle$ in z and Q^2 bins is given in Table 17 and in Table 18. The latter has been integrated over Q^2. Finally Table 19 contains the ratio of charge multiplicities in different bins of x and z. All errors quoted are statistical errors only.

The kinematic bins used for these tables are defined as follows in Tables 7 and 8:

Table 7. Kinematic bins for scaled energy distributions and charge multiplicity ratios

z_{Had}	x_{Bj}	W[GeV]	Q^2 [GeV^2]
0.10–0.15	0.01–0.02	6– 8	2 – 3
0.15–0.25	0.02–0.09	8–10	3 – 5
0.25–0.35	0.09–0.20	10–12	5 – 7.5
0.35–0.45	0.20–0.35	12–14	7.5– 11
0.45–0.60	0.35–0.40	14–16	11 – 16
0.60–1	0.4 –0.6	16–18	16 – 30
	0.6 –1	18–20	30 – 50
			50 –100
			100 –250

Table 8. p_t^2 bins for inclusive p_t^2 distributions

p_t^2 [GeV^2]				
0 –0.1875	0.1875–0.375	0.375 –0.5625	0.5625– 0.75	0.75 – 0.9375
0.9375–1.125	1.125 –1.3125	1.3125–1.5	1.5 – 2.0625	2.0625– 3.0
3.0 –3.9375	3.9375–5.625	5.625 –8.4375	8.4375–12.0	12.0 –16.0

Table 9. $\frac{1}{N_\mu}\cdot\frac{dN^{+(-)}}{dz}$ in bins of x and Q^2 for μp-scattering

Proton		dN/dz in bins of x and Q^2 (positive hadrons)					
$\langle x\rangle$	$\langle Q^2\rangle$	$0.10<z<0.15$	$0.15<z<0.25$	$0.25<z<0.35$	$0.35<z<0.45$	$0.45<z<0.60$	$0.60<z<1.0$
0.027	4.1	5.32±0.26	2.92±0.15	1.35±0.11	0.792±0.093	0.374±0.058	0.088±0.018
0.028	6.1	5.65±0.20	3.05±0.11	1.26±0.08	0.596±0.060	0.360±0.043	0.084±0.014
0.029	9.1	5.27±0.18	2.59±0.10	1.25±0.08	0.583±0.062	0.271±0.037	0.078±0.016
0.032	11.9	5.59±0.34	3.16±0.24	1.68±0.27	1.452±0.407	0.386±0.141	0.739±0.555
0.054	3.8	5.67±0.41	2.77±0.18	1.53±0.14	0.874±0.110	0.447±0.061	0.156±0.027
0.057	6.3	6.02±0.23	3.14±0.11	1.56±0.08	0.961±0.070	0.404±0.034	0.096±0.010
0.059	9.2	6.58±0.18	3.37±0.09	1.60±0.06	0.813±0.048	0.414±0.028	0.106±0.009
0.062	13.2	6.03±0.14	2.98±0.07	1.60±0.06	0.870±0.047	0.393±0.026	0.102±0.008
0.067	20.0	5.55±0.12	2.93±0.07	1.44±0.05	0.798±0.048	0.374±0.028	0.104±0.009
0.082	33.3	5.31±0.54	1.95±0.23	1.12±0.23	0.655±0.234	0.295±0.138	0.043±0.024
0.094	4.6	5.34±2.34	3.40±1.27	0.86±0.51	0.001±0.001	0.872±0.625	0.541±0.605
0.112	6.4	7.01±0.88	3.46±0.35	1.66±0.20	1.338±0.218	0.588±0.105	0.178±0.037
0.122	9.2	7.15±0.45	3.73±0.20	1.90±0.13	0.876±0.077	0.490±0.050	0.133±0.015
0.120	13.5	6.16±0.27	3.30±0.13	1.75±0.09	1.045±0.075	0.479±0.036	0.124±0.012
0.141	21.7	6.21±0.13	3.55±0.07	1.78±0.05	0.939±0.037	0.468±0.021	0.138±0.007
0.142	36.6	6.06±0.15	3.19±0.08	1.54±0.06	0.858±0.045	0.472±0.026	0.114±0.008
0.164	62.4	5.57±0.32	2.72±0.17	1.65±0.14	0.887±0.114	0.484±0.072	0.133±0.023
0.216	9.7	6.72±3.29	2.01±0.62	1.56±0.71	0.788±0.381	0.075±0.078	0.225±0.110
0.234	14.1	4.63±0.76	3.60±0.54	2.94±0.51	0.994±0.239	0.426±0.104	0.111±0.031
0.248	24.9	6.30±0.35	3.79±0.17	2.07±0.12	1.332±0.104	0.596±0.049	0.158±0.016
0.266	37.8	6.32±0.23	3.57±0.12	1.88±0.08	1.005±0.062	0.540±0.037	0.136±0.012
0.275	64.7	6.06±0.22	3.40±0.12	1.72±0.08	1.020±0.067	0.521±0.037	0.122±0.011
0.323	118.9	4.89±0.59	2.02±0.27	1.24±0.21	0.665±0.157	0.447±0.108	0.108±0.031
0.485	25.9	6.27±2.09	4.59±1.49	1.80±0.67	0.836±0.386	4.543±2.957	0.216±0.183
0.488	45.3	7.99±1.33	4.57±0.66	2.07±0.42	1.026±0.255	0.975±0.237	0.201±0.073
0.511	69.8	6.80±0.60	4.21±0.32	2.54±0.23	1.330±0.177	0.615±0.090	0.186±0.032
0.539	134.9	5.91±0.68	2.77±0.31	2.01±0.27	1.328±0.223	0.590±0.113	0.173±0.039

Proton		dN/dz in bins of x and Q^2 (negative hadrons)					
$\langle x\rangle$	$\langle Q^2\rangle$	$0.10<z<0.15$	$0.15<z<0.25$	$0.25<z<0.35$	$0.35<z<0.45$	$0.45<z<0.60$	$0.60<z<1.0$
0.027	4.1	4.65±0.23	2.31±0.12	1.19±0.09	0.421±0.055	0.211±0.032	0.047±0.010
0.028	6.1	5.11±0.18	2.49±0.09	1.14±0.06	0.596±0.051	0.234±0.026	0.060±0.010
0.029	9.1	4.37±0.15	2.32±0.08	1.04±0.06	0.552±0.051	0.251±0.031	0.056±0.010
0.032	11.9	4.53±0.27	2.44±0.16	1.52±0.18	0.583±0.116	0.305±0.083	0.107±0.043
0.054	3.8	4.51±0.34	2.60±0.18	0.99±0.10	0.534±0.074	0.287±0.048	0.071±0.013
0.057	6.3	5.09±0.21	2.56±0.10	1.06±0.06	0.563±0.046	0.270±0.027	0.062±0.008
0.059	9.2	5.49±0.16	2.77±0.08	1.21±0.05	0.629±0.042	0.271±0.022	0.065±0.007
0.062	13.2	5.02±0.12	2.40±0.06	1.15±0.04	0.585±0.035	0.268±0.020	0.055±0.006
0.067	20.0	4.69±0.11	2.46±0.06	1.09±0.04	0.518±0.034	0.246±0.021	0.049±0.006
0.082	33.3	4.13±0.42	2.09±0.24	1.12±0.22	0.275±0.101	0.191±0.096	0.027±0.024
0.094	4.6	4.15±2.48	1.27±0.56	2.36±1.43	0.436±0.229	0.020±0.018	0.068±0.050
0.112	6.4	5.22±0.70	2.99±0.37	1.25±0.22	0.523±0.120	0.387±0.094	0.057±0.018
0.122	9.2	5.43±0.38	2.67±0.16	1.31±0.10	0.583±0.068	0.316±0.043	0.051±0.010
0.120	13.5	5.19±0.24	2.51±0.10	1.09±0.07	0.518±0.045	0.237±0.025	0.047±0.006
0.141	21.7	5.34±0.12	2.54±0.05	1.15±0.04	0.520±0.027	0.235±0.015	0.047±0.004
0.142	36.6	5.13±0.13	2.38±0.07	0.99±0.04	0.458±0.031	0.219±0.018	0.035±0.004
0.164	62.4	4.45±0.26	2.27±0.15	1.02±0.11	0.538±0.084	0.222±0.043	0.049±0.012
0.216	9.7	8.06±5.04	4.23±2.03	1.21±0.60	0.398±0.238	0.546±0.839	0.149±0.149
0.234	14.1	4.92±0.97	2.86±0.49	0.81±0.21	0.668±0.231	0.158±0.057	0.058±0.027
0.248	24.9	4.95±0.27	2.64±0.13	1.13±0.08	0.561±0.060	0.255±0.030	0.031±0.006
0.266	37.8	4.85±0.20	2.53±0.09	1.10±0.06	0.552±0.045	0.205±0.022	0.024±0.004
0.275	64.7	4.67±0.18	2.40±0.09	0.97±0.06	0.417±0.040	0.185±0.021	0.030±0.005
0.323	118.9	4.17±0.53	1.94±0.26	1.02±0.19	0.627±0.163	0.162±0.063	0.090±0.030
0.485	25.9	2.99±1.58	2.10±0.87	2.34±1.11	0.356±0.278	0.234±0.285	0.020±0.018
0.488	45.3	4.04±0.74	2.53±0.46	1.28±0.30	0.442±0.145	0.306±0.122	0.030±0.018
0.511	69.8	5.75±0.51	2.47±0.22	1.05±0.14	0.488±0.094	0.217±0.054	0.050±0.015
0.539	134.9	4.52±0.56	1.92±0.25	0.67±0.15	0.410±0.129	0.099±0.045	0.037±0.019

Table 10. $\frac{1}{N_\mu}\cdot\frac{dN^{+(-)}}{dz}$ in bins of x and Q^2 for μd-scattering

Deuteron		dN/dz in bins of x and Q^2 (positive hadrons)					
$\langle x\rangle$	$\langle Q^2\rangle$	$0.10<z<0.15$	$0.15<z<0.25$	$0.25<z<0.35$	$0.35<z<0.45$	$0.45<z<0.60$	$0.60<z<1.0$
0.028	2.4	5.357±0.185	2.716±0.088	1.408±0.066	0.800±0.051	0.531±0.039	0.132±0.011
0.031	3.4	5.719±0.286	2.629±0.128	1.531±0.109	0.861±0.085	0.489±0.054	0.142±0.019
0.023	6.9	7.387±1.555	3.134±0.679	0.857±0.261	0.805±0.381	0.476±0.307	0.118±0.106
0.027	9.0	5.900±0.418	3.197±0.236	1.672±0.187	0.861±0.144	0.404±0.072	0.115±0.026
0.031	12.3	5.579±0.503	2.901±0.260	1.888±0.273	0.772±0.141	0.640±0.161	0.086±0.024
0.050	2.5	6.376±0.432	3.008±0.151	1.772±0.118	0.865±0.071	0.484±0.047	0.149±0.015
0.059	3.8	5.426±0.152	2.965±0.071	1.573±0.050	0.867±0.035	0.445±0.020	0.134±0.007
0.062	6.0	5.441±0.147	2.972±0.074	1.531±0.054	0.850±0.040	0.431±0.023	0.125±0.007
0.055	9.6	5.206±0.317	3.117±0.188	1.615±0.137	0.645±0.073	0.412±0.055	0.114±0.017
0.060	13.2	5.144±0.273	3.144±0.179	1.500±0.125	0.996±0.118	0.350±0.046	0.094±0.016
0.066	20.3	5.779±0.209	2.962±0.113	1.666±0.094	0.838±0.067	0.517±0.049	0.096±0.011
0.081	33.0	5.119±0.663	3.301±0.408	1.827±0.380	0.774±0.181	0.457±0.172	0.122±0.066
0.103	4.3	5.682±0.747	3.594±0.342	1.660±0.176	1.061±0.140	0.391±0.052	0.156±0.023
0.124	6.2	6.227±0.355	3.363±0.148	1.608±0.085	0.994±0.064	0.488±0.035	0.139±0.011
0.138	9.0	5.756±0.255	2.947±0.109	1.507±0.072	0.884±0.056	0.435±0.029	0.142±0.011
0.121	13.6	5.777±0.386	3.037±0.183	1.538±0.123	0.836±0.084	0.406±0.046	0.095±0.012
0.136	21.5	5.611±0.220	2.947±0.114	1.479±0.082	0.873±0.064	0.453±0.036	0.078±0.008
0.141	37.6	5.750±0.224	2.957±0.122	1.665±0.095	0.901±0.072	0.462±0.040	0.096±0.012
0.164	59.4	5.345±0.437	2.920±0.253	1.382±0.173	0.788±0.137	0.464±0.085	0.156±0.030
0.227	9.6	6.140±1.086	3.171±0.387	1.737±0.275	1.534±0.293	0.609±0.127	0.172±0.038
0.265	13.3	6.941±0.625	3.668±0.269	1.694±0.166	1.304±0.147	0.577±0.076	0.135±0.020
0.261	23.2	6.331±0.392	3.409±0.184	1.467±0.105	0.850±0.075	0.379±0.038	0.135±0.015
0.272	38.4	5.915±0.347	3.065±0.159	1.654±0.114	0.848±0.081	0.502±0.055	0.099±0.013
0.283	67.5	5.843±0.312	3.085±0.160	1.566±0.115	0.792±0.080	0.397±0.047	0.125±0.016
0.325	118.3	5.683±0.832	2.672±0.426	1.476±0.329	0.940±0.258	0.454±0.147	0.120±0.046
0.471	22.5	5.712±1.177	4.542±0.730	2.500±0.539	1.503±0.369	0.624±0.210	0.278±0.095
0.487	40.2	5.015±1.044	4.966±0.732	2.345±0.446	1.164±0.291	0.696±0.198	0.032±0.023
0.489	69.2	7.633±0.926	3.038±0.363	1.930±0.272	0.975±0.203	0.503±0.113	0.099±0.027
0.510	134.7	6.433±0.907	2.912±0.440	1.460±0.315	1.300±0.296	0.498±0.146	0.184±0.054

Deuteron		dN/dz in bins of x and Q^2 (negative hadrons)					
$\langle x\rangle$	$\langle Q^2\rangle$	$0.10<z<0.15$	$0.15<z<0.25$	$0.25<z<0.35$	$0.35<z<0.45$	$0.45<z<0.60$	$0.60<z<1.0$
0.028	2.4	4.730±0.171	2.357±0.079	1.279±0.064	0.660±0.047	0.316±0.027	0.090±0.009
0.031	3.4	4.549±0.232	2.364±0.119	1.122±0.087	0.728±0.080	0.296±0.036	0.105±0.017
0.023	6.9	6.697±1.553	2.550±0.636	0.759±0.264	1.744±1.281	0.100±0.062	0.206±0.253
0.027	9.0	5.926±0.446	3.037±0.268	1.568±0.210	0.608±0.116	0.268±0.054	0.080±0.022
0.031	12.3	4.668±0.466	2.536±0.275	1.780±0.303	0.698±0.164	0.208±0.061	0.106±0.033
0.050	2.5	5.241±0.357	2.331±0.122	1.152±0.077	0.619±0.055	0.325±0.033	0.101±0.012
0.059	3.8	4.770±0.135	2.587±0.064	1.181±0.041	0.655±0.031	0.279±0.015	0.084±0.005
0.062	6.0	6.409±0.129	2.471±0.066	1.166±0.047	0.624±0.035	0.326±0.021	0.082±0.006
0.055	9.6	4.694±0.292	2.363±0.150	1.062±0.104	0.577±0.077	0.261±0.045	0.065±0.014
0.060	13.2	4.924±0.278	2.529±0.155	1.028±0.095	0.617±0.084	0.370±0.063	0.064±0.014
0.066	20.3	4.896±0.193	2.535±0.112	1.326±0.092	0.635±0.064	0.299±0.035	0.063±0.010
0.081	33.0	4.453±0.653	2.446±0.395	1.699±0.369	0.556±0.197	0.447±0.159	0.050±0.029
0.103	4.3	4.353±0.557	2.304±0.214	1.352±0.156	0.639±0.097	0.313±0.052	0.099±0.019
0.124	6.2	4.678±0.259	2.429±0.112	1.291±0.078	0.675±0.054	0.328±0.029	0.078±0.008
0.138	9.0	4.962±0.220	2.562±0.100	1.103±0.060	0.653±0.047	0.268±0.023	0.055±0.006
0.121	13.6	4.581±0.299	2.197±0.144	1.110±0.099	0.510±0.064	0.258±0.039	0.049±0.008
0.136	21.5	4.668±0.194	2.469±0.105	1.056±0.068	0.510±0.047	0.230±0.025	0.042±0.006
0.141	37.6	4.726±0.204	2.778±0.125	1.256±0.087	0.562±0.057	0.232±0.032	0.050±0.008
0.164	59.4	4.199±0.383	2.858±0.238	1.174±0.174	0.559±0.121	0.320±0.075	0.079±0.025
0.227	9.6	4.534±0.761	2.805±0.359	1.206±0.202	0.462±0.115	0.254±0.067	0.079±0.027
0.265	13.3	4.313±0.434	2.605±0.214	1.427±0.150	0.597±0.088	0.291±0.049	0.054±0.012
0.261	23.2	5.101±0.348	2.372±0.140	1.120±0.098	0.449±0.049	0.267±0.036	0.048±0.008
0.272	38.4	4.729±0.289	2.764±0.154	1.059±0.092	0.630±0.075	0.237±0.041	0.026±0.006
0.283	67.5	4.703±0.273	2.364±0.137	1.201±0.101	0.528±0.067	0.243±0.038	0.043±0.010
0.325	118.3	4.485±0.744	2.715±0.442	0.693±0.223	0.460±0.177	0.630±0.206	0.064±0.033
0.471	22.5	3.463±0.925	2.813±0.537	0.898±0.245	0.607±0.230	0.314±0.167	0.061±0.037
0.487	40.2	4.245±0.921	2.583±0.445	0.938±0.237	0.731±0.229	0.619±0.191	0.018±0.018
0.489	69.2	5.357±0.705	2.664±0.318	1.223±0.218	0.440±0.128	0.158±0.062	0.022±0.013
0.510	134.7	5.698±0.845	1.576±0.325	0.710±0.216	0.833±0.226	0.288±0.110	0.015±0.015

Table 11. $\frac{1}{N_\mu}\cdot\frac{dN^{charged}}{dz}$ in bins of x and Q^2 for μp- and μd-scattering

Proton		dN/dz in bins of x and Q^2 (charged hadrons)					
$\langle x\rangle$	$\langle Q^2\rangle$	$0.10<z<0.15$	$0.15<z<0.25$	$0.25<z<0.35$	$0.35<z<0.45$	$0.45<z<0.60$	$0.60<z<1.0$
0.027	4.1	9.97±0.35	5.21±0.19	2.54±0.14	1.184±0.103	0.563±0.061	0.129±0.019
0.028	6.1	10.77±0.27	5.52±0.14	2.40±0.10	1.206±0.079	0.583±0.048	0.146±0.017
0.029	9.1	9.61±0.23	4.91±0.13	2.29±0.10	1.145±0.080	0.526±0.048	0.138±0.018
0.032	11.9	10.07±0.43	5.49±0.28	3.17±0.31	1.683±0.271	0.688±0.150	0.411±0.137
0.054	3.8	10.18±0.54	5.38±0.26	2.52±0.17	1.391±0.129	0.734±0.078	0.224±0.029
0.057	6.3	11.12±0.31	5.69±0.15	2.62±0.10	1.502±0.082	0.673±0.043	0.159±0.013
0.059	9.2	12.07±0.25	6.14±0.12	2.81±0.08	1.442±0.063	0.684±0.035	0.171±0.011
0.062	13.2	11.03±0.18	5.38±0.09	2.76±0.07	1.448±0.058	0.661±0.033	0.155±0.010
0.067	20.0	10.23±0.16	5.39±0.09	2.52±0.07	1.302±0.057	0.617±0.034	0.152±0.011
0.082	33.3	9.43±0.68	4.06±0.34	2.26±0.33	0.862±0.218	0.486±0.167	0.071±0.034
0.094	4.6	9.55±3.39	4.46±1.26	3.01±1.25	2.807±1.550	2.341±1.724	0.385±0.238
0.112	6.4	12.27±1.13	6.42±0.51	2.88±0.29	1.864±0.246	0.975±0.140	0.234±0.041
0.122	9.2	12.58±0.59	6.40±0.25	3.22±0.17	1.461±0.103	0.804±0.066	0.184±0.018
0.120	13.5	11.35±0.36	5.81±0.16	2.84±0.11	1.542±0.085	0.716±0.044	0.169±0.013
0.141	21.7	11.56±0.18	6.08±0.09	2.94±0.06	1.461±0.046	0.704±0.025	0.183±0.008
0.142	36.6	11.20±0.20	5.57±0.10	2.53±0.07	1.311±0.054	0.693±0.032	0.150±0.009
0.164	62.4	10.01±0.41	5.00±0.22	2.66±0.18	1.419±0.141	0.692±0.082	0.179±0.025
0.216	9.7	13.96±5.23	4.80±1.19	2.78±0.94	1.190±0.456	0.231±0.177	0.390±0.175
0.234	14.1	9.33±1.17	6.46±0.73	3.72±0.54	1.644±0.323	0.581±0.117	0.167±0.039
0.248	24.9	11.30±0.44	6.42±0.22	3.20±0.15	1.879±0.118	0.849±0.057	0.180±0.016
0.266	37.8	11.17±0.31	6.10±0.15	2.98±0.10	1.557±0.076	0.746±0.043	0.157±0.012
0.275	64.7	10.72±0.29	5.79±0.15	2.70±0.10	1.423±0.077	0.702±0.042	0.151±0.012
0.323	118.9	9.08±0.79	3.98±0.38	2.27±0.29	1.272±0.222	0.605±0.124	0.196±0.042
0.485	25.9	9.27±2.62	6.67±1.70	3.92±1.15	1.212±0.482	4.043±2.194	0.189±0.151
0.488	45.3	11.66±1.43	7.06±0.79	3.37±0.51	1.455±0.288	1.280±0.265	0.219±0.069
0.511	69.8	12.61±0.79	6.64±0.38	3.59±0.27	1.797±0.196	0.837±0.105	0.233±0.035
0.539	134.9	10.42±0.88	4.69±0.39	2.66±0.31	1.725±0.256	0.683±0.120	0.209±0.044
Deuteron		dN/dz in bins of x and Q^2 (charged hadrons)					
$\langle x\rangle$	$\langle Q^2\rangle$	$0.10<z<0.15$	$0.15<z<0.25$	$0.25<z<0.35$	$0.35<z<0.45$	$0.45<z<0.60$	$0.60<z<1.0$
0.028	2.4	10.086±0.252	5.073±0.118	2.688±0.092	1.461±0.069	0.844±0.046	0.222±0.014
0.031	3.4	10.230±0.365	4.994±0.175	2.644±0.138	1.589±0.116	0.774±0.063	0.246±0.026
0.023	6.9	14.077±2.194	5.697±0.932	1.617±0.371	2.058±0.803	0.415±0.177	0.298±0.213
0.027	9.0	11.829±0.610	6.224±0.353	3.220±0.276	1.467±0.185	0.670±0.089	0.195±0.034
0.031	12.3	10.279±0.688	5.436±0.375	3.641±0.401	1.465±0.212	0.796±0.149	0.190±0.039
0.050	2.5	11.607±0.558	5.329±0.194	2.885±0.136	1.481±0.089	0.803±0.057	0.250±0.019
0.059	3.8	10.195±0.203	5.552±0.096	2.751±0.064	1.522±0.047	0.723±0.025	0.218±0.009
0.062	6.0	10.043±0.195	5.440±0.099	2.698±0.072	1.476±0.053	0.755±0.031	0.207±0.010
0.055	9.6	9.902±0.431	5.466±0.239	2.680±0.171	1.218±0.105	0.675±0.071	0.181±0.022
0.060	13.2	10.064±0.389	5.673±0.236	2.523±0.156	1.604±0.143	0.704±0.073	0.158±0.021
0.066	20.3	10.685±0.285	5.501±0.159	2.995±0.131	1.470±0.092	0.817±0.060	0.159±0.015
0.081	33.0	9.576±0.930	5.857±0.576	3.533±0.531	1.333±0.261	0.932±0.239	0.161±0.063
0.103	4.3	9.988±0.916	5.798±0.385	3.017±0.236	1.694±0.168	0.701±0.073	0.256±0.030
0.124	6.2	10.872±0.432	5.764±0.183	2.898±0.116	1.669±0.083	0.817±0.046	0.217±0.014
0.138	9.0	10.716±0.336	5.513±0.148	2.608±0.093	1.537±0.073	0.704±0.037	0.195±0.012
0.121	13.6	10.317±0.481	5.223±0.231	2.647±0.158	1.347±0.106	0.663±0.060	0.144±0.015
0.136	21.5	10.280±0.293	5.416±0.155	2.534±0.106	1.382±0.079	0.683±0.044	0.120±0.010
0.141	37.6	10.484±0.303	5.723±0.174	2.921±0.129	1.463±0.092	0.702±0.052	0.147±0.015
0.164	59.4	9.543±0.581	5.506±0.347	2.546±0.243	1.344±0.182	0.781±0.112	0.235±0.039
0.227	9.6	10.782±1.314	6.006±0.530	2.938±0.338	1.883±0.280	0.842±0.137	0.251±0.047
0.265	13.3	11.155±0.747	6.267±0.343	3.129±0.224	1.882±0.168	0.865±0.089	0.189±0.023
0.261	23.2	11.419±0.524	5.758±0.230	2.587±0.144	1.294±0.088	0.643±0.052	0.181±0.017
0.272	38.4	10.623±0.450	5.830±0.222	2.715±0.146	1.469±0.110	0.745±0.069	0.125±0.014
0.283	67.5	10.537±0.414	5.446±0.210	2.766±0.153	1.319±0.104	0.638±0.060	0.169±0.019
0.325	118.3	10.173±1.116	5.374±0.612	2.166±0.397	1.399±0.313	1.026±0.232	0.185±0.057
0.471	22.5	9.178±1.498	7.339±0.903	3.211±0.541	2.112±0.434	0.941±0.268	0.325±0.096
0.487	40.2	9.299±1.395	7.411±0.828	3.198±0.483	1.894±0.370	1.324±0.276	0.049±0.029
0.489	69.2	12.931±1.153	5.728±0.484	3.154±0.349	1.405±0.238	0.660±0.129	0.121±0.030
0.510	134.7	12.130±1.240	4.493±0.547	2.165±0.381	2.138±0.373	0.786±0.183	0.197±0.055

Table 12. $\frac{1}{N_\mu}\cdot\frac{dN^{+(-)}}{dz}$ in bins of W and Q^2 for μp-scattering

Proton		dN/dz in bins of W and Q^2 (positive hadrons)					
$\langle W\rangle$	$\langle Q^2\rangle$	$0.10<z<0.15$	$0.15<z<0.25$	$0.25<z<0.35$	$0.35<z<0.45$	$0.45<z<0.60$	$0.60<z<1.0$
7.3	3.4	5.681±1.716	2.982±0.782	1.526±0.536	0.942±0.365	0.468±0.230	0.582±0.381
7.1	6.4	7.063±0.624	3.266±0.238	1.633±0.149	1.268±0.145	0.565±0.070	0.179±0.026
7.3	14.2	5.803±0.533	3.742±0.289	1.791±0.173	1.146±0.139	0.546±0.073	0.177±0.027
7.2	36.9	6.350±0.654	3.486±0.307	2.035±0.219	0.924±0.141	0.694±0.104	0.113±0.025
7.3	75.3	8.449±1.372	3.702±0.568	2.750±0.474	1.638±0.363	0.656±0.175	0.167±0.061
9.1	3.5	4.619±0.648	2.802±0.340	1.178±0.195	0.718±0.186	0.826±0.219	0.136±0.041
9.0	6.9	6.199±0.297	3.350±0.141	1.770±0.099	0.857±0.066	0.481±0.040	0.117±0.012
9.2	14.9	5.865±0.260	3.310±0.126	1.653±0.083	1.048±0.069	0.437±0.032	0.116±0.010
9.3	28.8	6.320±0.317	2.794±0.166	2.063±0.113	1.268±0.093	0.604±0.049	0.166±0.016
9.1	71.0	5.131±0.504	3.254±0.274	1.869±0.204	1.078±0.163	0.576±0.092	0.158±0.029
10.9	3.5	5.277±0.501	2.957±0.301	1.570±0.220	0.948±0.202	0.333±0.100	0.060±0.025
10.8	7.2	6.753±0.248	3.159±0.113	1.514±0.079	0.938±0.067	0.426±0.035	0.109±0.011
10.8	13.9	6.347±0.255	3.529±0.132	1.745±0.092	0.942±0.066	0.440±0.034	0.138±0.013
11.0	29.9	6.557±0.220	3.460±0.111	1.879±0.081	0.950±0.055	0.469±0.030	0.134±0.011
11.1	87.3	6.079±0.401	3.312±0.201	2.029±0.158	1.020±0.113	0.626±0.070	0.093±0.016
12.7	3.6	4.645±0.463	3.048±0.314	1.077±0.181	0.733±0.219	0.388±0.125	0.121±0.059
13.1	6.3	5.701±0.204	3.194±0.113	1.658±0.088	0.831±0.066	0.374±0.036	0.111±0.013
12.9	14.5	6.298±0.206	3.315±0.109	1.667±0.078	0.875±0.056	0.486±0.036	0.114±0.010
13.0	28.8	6.538±0.197	3.652±0.107	1.806±0.075	0.934±0.052	0.522±0.031	0.129±0.010
12.9	65.1	6.023±0.339	3.552±0.188	1.503±0.115	1.046±0.100	0.454±0.051	0.135±0.018
15.0	7.0	5.739±0.211	3.117±0.123	1.439±0.091	0.835±0.077	0.398±0.044	0.106±0.016
14.9	13.9	6.068±0.196	3.175±0.105	1.661±0.082	0.781±0.055	0.348±0.030	0.091±0.009
15.2	29.3	6.147±0.188	3.504±0.108	1.773±0.079	0.962±0.060	0.494±0.034	0.123±0.011
14.8	82.8	6.026±0.350	2.980±0.184	1.822±0.145	0.919±0.100	0.489±0.060	0.135±0.019
17.1	7.9	5.526±0.235	3.047±0.141	1.304±0.108	0.560±0.071	0.323±0.052	0.102±0.023
17.1	13.8	5.674±0.193	2.958±0.108	1.529±0.090	0.862±0.075	0.384±0.042	0.117±0.017
16.8	30.4	5.407±0.187	2.862±0.104	1.385±0.081	0.772±0.062	0.395±0.038	0.110±0.012
17.0	78.7	5.103±0.345	2.499±0.180	1.415±0.147	0.641±0.097	0.416±0.066	0.116±0.020
18.9	7.6	5.699±0.435	2.777±0.267	1.872±0.293	1.041±0.292	0.563±0.261	0.120±0.080
18.6	12.8	5.371±0.220	2.573±0.125	1.488±0.135	1.040±0.160	0.335±0.061	0.165±0.049
19.1	28.5	5.916±0.254	2.814±0.151	1.417±0.141	1.129±0.182	0.809±0.169	0.144±0.039
19.1	66.7	5.497±0.552	2.600±0.294	1.743±0.290	1.359±0.307	0.484±0.157	0.143±0.055

Proton		dN/dz in bins of W and Q^2 (negative hadrons)					
$\langle W\rangle$	$\langle Q^2\rangle$	$0.10<z<0.15$	$0.15<z<0.25$	$0.25<z<0.35$	$0.35<z<0.45$	$0.45<z<0.60$	$0.60<z<1.0$
7.3	3.4	2.959±1.075	3.502±1.063	1.371±0.541	0.425±0.166	0.694±0.399	0.080±0.057
7.1	6.4	5.496±0.535	2.658±0.225	1.360±0.159	0.573±0.080	0.333±0.058	0.070±0.013
7.3	14.2	5.121±0.511	2.798±0.244	1.068±0.134	0.498±0.086	0.181±0.042	0.053±0.014
7.2	36.9	4.208±0.452	2.507±0.245	1.078±0.147	0.432±0.090	0.291±0.064	0.036±0.012
7.3	75.3	6.454±1.063	2.328±0.390	1.080±0.282	0.477±0.186	0.295±0.125	0.082±0.040
9.1	3.5	4.977±0.702	2.477±0.311	1.387±0.271	0.487±0.131	0.296±0.083	0.067±0.021
9.0	6.9	4.660±0.238	2.323±0.110	1.106±0.074	0.673±0.060	0.252±0.028	0.050±0.007
9.2	14.9	4.825±0.223	2.519±0.104	1.042±0.066	0.547±0.047	0.207±0.020	0.047±0.007
9.3	28.8	4.716±0.244	2.798±0.134	1.160±0.083	0.618±0.063	0.249±0.030	0.042±0.007
9.1	71.0	4.551±0.471	1.998±0.200	0.854±0.141	0.531±0.107	0.174±0.047	0.030±0.012
10.9	3.5	4.801±0.462	2.300±0.234	1.193±0.186	0.545±0.122	0.222±0.057	0.062±0.024
10.8	7.2	5.219±0.206	2.742±0.103	1.105±0.064	0.526±0.044	0.311±0.030	0.061±0.008
10.8	13.9	5.436±0.236	2.605±0.107	1.110±0.069	0.568±0.050	0.241±0.025	0.049±0.006
11.0	29.9	5.086±0.183	2.524±0.090	1.200±0.064	0.469±0.037	0.204±0.019	0.032±0.004
11.1	87.3	4.126±0.301	2.229±0.162	0.898±0.097	0.407±0.067	0.109±0.025	0.023±0.008
12.7	3.6	4.771±0.441	2.399±0.247	1.003±0.172	0.436±0.118	0.241±0.077	0.045±0.015
13.1	6.3	5.112±0.187	2.559±0.096	1.232±0.067	0.670±0.055	0.223±0.024	0.059±0.009
12.9	14.5	5.175±0.181	2.528±0.089	1.170±0.064	0.554±0.043	0.270±0.026	0.056±0.007
13.0	28.8	5.631±0.181	2.596±0.088	1.134±0.059	0.525±0.037	0.249±0.022	0.036±0.005
12.9	65.1	4.668±0.281	2.397±0.148	0.968±0.094	0.354±0.053	0.190±0.032	0.034±0.009
15.0	7.0	5.265±0.198	2.801±0.107	1.197±0.072	0.546±0.050	0.272±0.030	0.062±0.010
14.9	13.9	5.337±0.179	2.635±0.093	1.241±0.070	0.556±0.045	0.329±0.032	0.057±0.008
15.2	29.3	5.257±0.169	2.495±0.087	1.164±0.064	0.614±0.049	0.222±0.022	0.039±0.006
14.8	82.8	4.696±0.296	2.288±0.159	0.934±0.099	0.505±0.074	0.208±0.040	0.039±0.009
17.1	7.9	4.849±0.204	2.287±0.103	1.128±0.082	0.552±0.061	0.228±0.032	0.049±0.010
17.1	13.8	4.787±0.162	2.315±0.087	1.092±0.067	0.538±0.049	0.256±0.031	0.056±0.009
16.8	30.4	4.710±0.168	2.331±0.092	0.901±0.060	0.432±0.043	0.236±0.029	0.042±0.007
17.0	78.7	4.390±0.305	2.151±0.164	1.061±0.123	0.455±0.083	0.206±0.044	0.067±0.016
18.9	7.6	4.345±0.317	2.719±0.220	1.208±0.180	0.680±0.143	0.441±0.130	0.135±0.059
18.6	12.8	4.448±0.178	2.300±0.106	1.263±0.100	0.586±0.072	0.248±0.041	0.092±0.025
19.1	28.5	4.609±0.196	2.463±0.121	1.154±0.103	0.518±0.072	0.231±0.045	0.048±0.014
19.1	66.7	4.800±0.465	2.407±0.268	0.980±0.185	0.568±0.161	0.218±0.081	0.015±0.011

Table 13. $\frac{1}{N_\mu}\cdot\frac{dN^{+(-)}}{dz}$ in bins of W and Q^2 for μd-scattering

Deuteron		dN/dz in bins of W and Q^2 (positive hadrons)					
$\langle W\rangle$	$\langle Q^2\rangle$	$0.10<z<0.15$	$0.15<z<0.25$	$0.25<z<0.35$	$0.35<z<0.45$	$0.45<z<0.60$	$0.60<z<1.0$
7.0	2.8	6.096±0.334	3.084±0.126	1.808±0.095	0.838±0.052	0.460±0.032	0.155±0.012
7.0	6.0	6.127±0.242	3.315±0.101	1.568±0.058	1.000±0.046	0.466±0.023	0.130±0.007
7.0	13.4	6.128±0.366	3.535±0.170	1.674±0.106	1.099±0.086	0.517±0.044	0.151±0.014
7.1	28.6	5.616±0.572	3.449±0.286	1.789±0.184	0.851±0.124	0.395±0.068	0.124±0.024
7.3	69.1	5.906±1.691	2.434±0.654	1.539±0.511	1.546±0.527	0.527±0.277	0.060±0.043
8.9	2.8	5.394±0.158	2.768±0.073	1.398±0.051	0.816±0.040	0.491±0.027	0.132±0.009
8.9	6.1	5.563±0.147	2.909±0.068	1.487±0.047	0.808±0.034	0.417±0.020	0.125±0.007
9.3	14.4	6.032±0.406	2.947±0.171	1.417±0.106	0.843±0.080	0.383±0.041	0.105±0.014
9.2	30.4	6.503±0.473	3.346±0.223	1.385±0.120	0.839±0.090	0.436±0.055	0.098±0.014
9.1	68.6	6.831±0.954	3.339±0.436	1.581±0.268	0.906±0.212	0.456±0.106	0.133±0.034
10.4	2.8	5.298±0.187	2.798±0.099	1.591±0.086	0.840±0.062	0.465±0.039	0.126±0.013
10.9	6.4	5.351±0.155	2.740±0.078	1.654±0.067	0.836±0.048	0.432±0.028	0.124±0.009
11.0	14.4	5.782±0.415	2.855±0.198	1.745±0.177	0.901±0.122	0.377±0.053	0.095±0.017
11.0	29.0	5.081±0.295	2.992±0.155	1.583±0.112	0.903±0.085	0.434±0.047	0.065±0.010
11.1	72.6	5.757±0.534	3.353±0.294	1.599±0.190	0.915±0.143	0.401±0.078	0.116±0.025
12.9	8.5	4.849±0.923	3.388±0.595	1.727±0.504	0.910±0.338	0.479±0.201	0.156±0.069
13.0	14.0	5.238±0.448	2.903±0.252	1.290±0.172	0.892±0.157	0.385±0.075	0.140±0.049
13.0	29.4	5.609±0.279	3.000±0.151	1.446±0.104	0.793±0.077	0.514±0.055	0.101±0.014
13.0	75.7	6.938±0.546	2.814±0.227	1.619±0.179	0.752±0.122	0.352±0.070	0.119±0.025
15.1	8.7	4.034±0.869	4.373±1.218	3.006±1.277	0.627±0.363	0.596±0.510	0.103±0.067
15.0	13.8	5.798±0.436	2.990±0.239	1.624±0.188	0.903±0.141	0.357±0.066	0.074±0.017
15.0	29.7	5.636±0.270	2.974±0.150	1.577±0.115	0.959±0.098	0.438±0.053	0.092±0.015
15.0	77.6	5.427±0.453	2.993±0.251	1.470±0.179	0.772±0.132	0.471±0.086	0.121±0.027
17.1	7.8	5.814±0.752	3.327±0.449	1.271±0.255	1.053±0.361	0.527±0.195	0.172±0.098
17.0	13.8	5.381±0.331	2.736±0.177	1.500±0.146	0.794±0.109	0.410±0.063	0.105±0.021
17.0	30.1	5.645±0.292	3.161±0.176	1.797±0.144	0.763±0.085	0.461±0.052	0.082±0.012
17.0	75.6	5.689±0.519	2.812±0.274	1.651±0.218	0.712±0.141	0.388±0.083	0.176±0.038
19.0	7.1	6.107±0.487	3.122±0.253	1.691±0.217	0.915±0.163	0.367±0.076	0.112±0.028
19.0	13.8	5.347±0.315	3.301±0.197	1.618±0.151	0.961±0.119	0.472±0.076	0.095±0.019
18.9	29.9	5.909±0.353	2.957±0.181	1.676±0.151	0.780±0.092	0.573±0.085	0.105±0.024
18.7	66.4	4.805±0.663	3.182±0.435	1.056±0.253	1.115±0.272	0.741±0.187	0.185±0.056

Deuteron		dN/dz in bins of W and Q^2 (negative hadrons)					
$\langle W\rangle$	$\langle Q^2\rangle$	$0.10<z<0.15$	$0.15<z<0.25$	$0.25<z<0.35$	$0.35<z<0.45$	$0.45<z<0.60$	$0.60<z<1.0$
7.0	2.8	5.059±0.277	2.462±0.103	1.171±0.062	0.647±0.046	0.304±0.023	0.097±0.009
7.0	6.0	4.673±0.179	2.388±0.075	1.227±0.051	0.631±0.034	0.299±0.019	0.074±0.005
7.0	13.4	4.534±0.282	2.426±0.131	1.298±0.091	0.595±0.058	0.222±0.027	0.047±0.007
7.1	28.6	4.607±0.491	2.622±0.232	1.005±0.131	0.545±0.095	0.331±0.064	0.044±0.013
7.3	69.1	4.320±1.378	2.957±0.699	1.264±0.477	0.799±0.343	0.199±0.146	0.061±0.044
8.9	2.8	4.866±0.148	2.509±0.069	1.227±0.049	0.653±0.036	0.336±0.022	0.087±0.007
8.9	6.1	4.799±0.132	2.542±0.063	1.197±0.043	0.680±0.034	0.279±0.016	0.070±0.005
9.3	14.4	5.046±0.334	2.446±0.158	1.032±0.091	0.504±0.058	0.246±0.035	0.050±0.008
9.2	30.4	4.944±0.380	2.487±0.172	0.919±0.100	0.516±0.066	0.220±0.038	0.032±0.007
9.1	68.6	4.288±0.655	2.228±0.308	1.002±0.214	0.364±0.121	0.171±0.068	0.019±0.014
10.4	2.8	4.627±0.172	2.316±0.086	1.184±0.066	0.671±0.055	0.281±0.027	0.102±0.012
10.9	6.4	4.522±0.133	2.445±0.074	1.119±0.052	0.612±0.042	0.317±0.024	0.088±0.009
11.0	14.4	4.662±0.344	2.104±0.153	0.961±0.101	0.481±0.073	0.269±0.051	0.056±0.013
11.0	29.0	4.933±0.297	2.631±0.156	1.055±0.098	0.535±0.069	0.239±0.042	0.033±0.007
11.1	72.6	5.394±0.525	2.589±0.250	1.032±0.152	0.657±0.133	0.216±0.054	0.025±0.011
12.9	8.5	4.113±0.716	2.341±0.472	0.675±0.209	0.620±0.290	0.339±0.198	0.085±0.052
13.0	14.0	4.166±0.381	2.260±0.215	1.074±0.157	0.395±0.082	0.308±0.088	0.053±0.019
13.0	29.4	4.799±0.257	2.568±0.143	1.068±0.088	0.525±0.066	0.237±0.034	0.035±0.007
13.0	75.7	4.304±0.396	2.364±0.214	1.305±0.166	0.635±0.116	0.288±0.066	0.041±0.014
15.1	8.7	4.846±1.157	1.937±0.454	1.197±0.556	0.729±0.422	0.344±0.249	0.107±0.128
15.0	13.8	5.078±0.383	2.932±0.257	1.003±0.133	0.599±0.118	0.285±0.066	0.044±0.012
15.0	29.7	4.336±0.229	2.549±0.145	1.519±0.130	0.528±0.070	0.284±0.046	0.065±0.013
15.0	77.6	5.285±0.458	2.211±0.211	1.070±0.152	0.379±0.089	0.345±0.085	0.076±0.024
17.1	7.8	7.114±0.974	3.522±0.578	1.489±0.387	0.533±0.194	0.270±0.118	0.190±0.132
17.0	13.8	4.678±0.312	2.805±0.219	1.325±0.158	0.813±0.145	0.320±0.060	0.049±0.014
17.0	30.1	4.723±0.259	2.638±0.162	1.116±0.110	0.655±0.094	0.293±0.053	0.063±0.013
17.0	75.6	4.270±0.442	2.413±0.250	1.188±0.197	0.473±0.121	0.255±0.070	0.063±0.023
19.0	7.1	5.524±0.480	3.127±0.307	1.210±0.165	0.790±0.154	0.248±0.053	0.078±0.022
19.0	13.8	5.107±0.338	2.438±0.173	1.609±0.182	0.619±0.099	0.301±0.056	0.104±0.024
18.9	29.9	5.136±0.341	2.552±0.186	1.294±0.136	0.634±0.100	0.206±0.044	0.082±0.020
18.7	66.4	4.138±0.610	2.811±0.433	1.091±0.282	0.668±0.215	0.453±0.161	0.057±0.036

Table 14. $\frac{1}{N_\mu}\cdot\frac{dN^{charged}}{dz}$ in bins of W and Q^2 for μp- and μd-scattering

Proton		dN/dz in bins of W and Q^2 (charged hadrons)					
$\langle W\rangle$	$\langle Q^2\rangle$	$0.10<z<0.15$	$0.15<z<0.25$	$0.25<z<0.35$	$0.35<z<0.45$	$0.45<z<0.60$	$0.60<z<1.0$
7.3	3.4	8.579±1.991	6.309±1.244	2.875±0.751	1.287±0.351	1.124±0.417	0.508±0.234
7.1	6.4	12.596±0.824	5.920±0.327	2.970±0.213	1.807±0.159	0.898±0.091	0.247±0.028
7.3	14.2	10.959±0.740	6.543±0.378	2.861±0.219	1.642±0.162	0.736±0.085	0.229±0.030
7.2	36.9	10.517±0.783	6.004±0.393	3.098±0.262	1.349±0.166	0.983±0.122	0.148±0.028
7.3	75.3	14.953±1.729	6.015±0.681	3.797±0.546	2.110±0.406	0.963±0.218	0.257±0.076
9.1	3.5	9.579±0.952	5.282±0.461	2.505±0.316	1.199±0.224	1.039±0.199	0.202±0.045
9.0	6.9	10.841±0.379	5.656±0.178	2.869±0.124	1.529±0.089	0.732±0.048	0.167±0.014
9.2	14.9	10.700±0.343	5.830±0.163	2.697±0.106	1.587±0.083	0.642±0.038	0.164±0.012
9.3	28.8	11.007±0.396	6.588±0.213	3.228±0.140	1.889±0.112	0.851±0.057	0.204±0.017
9.1	71.0	9.685±0.690	5.235±0.337	2.730±0.248	1.606±0.194	0.746±0.103	0.186±0.031
10.9	3.5	10.077±0.681	5.241±0.378	2.763±0.288	1.460±0.225	0.538±0.105	0.122±0.035
10.8	7.2	11.951±0.321	5.906±0.153	2.614±0.101	1.449±0.079	0.738±0.046	0.170±0.014
10.8	13.9	11.784±0.347	6.126±0.169	2.852±0.115	1.513±0.083	0.684±0.043	0.184±0.014
11.0	29.9	11.632±0.286	5.978±0.142	3.080±0.103	1.416±0.066	0.672±0.035	0.160±0.011
11.1	87.3	10.131±0.495	5.538±0.258	2.901±0.183	1.411±0.130	0.714±0.071	0.116±0.017
12.7	3.6	9.462±0.643	5.398±0.393	2.102±0.253	1.129±0.227	0.614±0.139	0.144±0.041
13.1	6.3	10.818±0.277	5.743±0.148	2.873±0.109	1.500±0.085	0.590±0.043	0.169±0.015
12.9	14.5	11.470±0.274	5.831±0.140	2.838±0.101	1.429±0.071	0.757±0.044	0.170±0.013
13.0	28.8	12.173±0.267	6.248±0.138	2.944±0.096	1.458±0.064	0.776±0.039	0.163±0.010
12.9	65.1	10.674±0.439	5.939±0.239	2.473±0.148	1.380±0.111	0.644±0.060	0.172±0.020
15.0	7.0	11.006±0.289	5.917±0.162	2.631±0.115	1.354±0.088	0.662±0.052	0.167±0.018
14.9	13.9	11.406±0.265	5.808±0.140	2.901±0.108	1.334±0.071	0.673±0.044	0.148±0.012
15.2	29.3	11.404±0.253	5.988±0.138	2.943±0.102	1.576±0.078	0.717±0.041	0.163±0.012
14.8	82.8	10.712±0.457	5.267±0.243	2.747±0.175	1.426±0.124	0.696±0.072	0.172±0.021
17.1	7.9	10.363±0.310	5.261±0.169	2.438±0.133	1.125±0.094	0.538±0.057	0.143±0.022
17.1	13.8	10.430±0.250	5.256±0.138	2.601±0.111	1.377±0.086	0.636±0.052	0.168±0.018
16.8	30.4	10.115±0.251	5.192±0.139	2.278±0.100	1.198±0.074	0.631±0.047	0.151±0.014
17.0	78.7	9.501±0.460	4.655±0.244	2.479±0.192	1.096±0.127	0.618±0.078	0.183±0.026
18.9	7.6	9.924±0.523	5.546±0.344	3.029±0.327	1.612±0.271	1.007±0.251	0.302±0.110
18.6	12.8	9.810±0.281	4.876±0.163	2.725±0.163	1.501±0.144	0.573±0.070	0.246±0.049
19.1	28.5	10.456±0.316	5.286±0.192	2.567±0.171	1.486±0.155	0.870±0.121	0.175±0.035
19.1	66.7	10.318±0.720	5.022±0.398	2.659±0.331	1.845±0.325	0.677±0.165	0.129±0.043

Deuteron		dN/dz in bins of W and Q^2 (charged hadrons)					
$\langle W\rangle$	$\langle Q^2\rangle$	$0.10<z<0.15$	$0.15<z<0.25$	$0.25<z<0.35$	$0.35<z<0.45$	$0.45<z<0.60$	$0.60<z<1.0$
7.0	2.8	11.146±0.432	5.537±0.162	2.941±0.110	1.485±0.069	0.762±0.039	0.251±0.015
7.0	6.0	10.745±0.296	5.671±0.124	2.795±0.078	1.628±0.057	0.765±0.030	0.204±0.009
7.0	13.4	10.605±0.457	5.940±0.213	2.974±0.140	1.684±0.103	0.735±0.051	0.195±0.016
7.1	28.6	10.245±0.754	6.067±0.368	2.780±0.224	1.397±0.157	0.726±0.093	0.167±0.027
7.3	69.1	10.215±2.176	5.454±0.966	2.800±0.697	2.336±0.624	0.712±0.304	0.121±0.062
8.9	2.8	10.260±0.217	5.278±0.100	2.625±0.071	1.470±0.054	0.828±0.035	0.219±0.011
8.9	6.1	10.361±0.197	5.452±0.092	2.684±0.064	1.485±0.048	0.696±0.026	0.195±0.008
9.3	14.4	11.067±0.523	5.393±0.233	2.449±0.140	1.346±0.098	0.630±0.054	0.155±0.016
9.2	30.4	11.394±0.602	5.822±0.280	2.300±0.157	1.355±0.112	0.655±0.067	0.129±0.016
9.1	68.6	10.957±1.128	5.508±0.523	2.585±0.343	1.248±0.238	0.631±0.126	0.157±0.038
10.4	2.8	9.925±0.054	5.110±0.131	2.759±0.107	1.511±0.083	0.742±0.047	0.228±0.017
10.9	6.4	9.860±0.204	5.185±0.108	2.772±0.085	1.448±0.064	0.749±0.037	0.212±0.013
11.0	14.4	10.425±0.536	4.944±0.249	2.649±0.193	1.368±0.138	0.646±0.073	0.151±0.021
11.0	29.0	10.011±0.418	5.614±0.219	2.648±0.149	1.439±0.110	0.678±0.063	0.098±0.012
11.1	72.6	11.148±0.749	5.937±0.386	2.631±0.244	1.566±0.194	0.618±0.095	0.141±0.028
12.9	8.5	8.953±1.155	5.740±0.761	2.313±0.487	1.530±0.446	0.816±0.278	0.243±0.088
13.0	14.0	9.427±0.588	5.161±0.331	2.364±0.233	1.248±0.167	0.685±0.111	0.181±0.045
13.0	29.4	10.410±0.379	5.568±0.208	2.514±0.136	1.319±0.102	0.749±0.064	0.134±0.016
13.0	75.7	11.136±0.664	5.176±0.312	2.921±0.244	1.386±0.167	0.641±0.096	0.160±0.029
15.1	8.7	8.816±1.410	5.737±1.021	4.093±1.269	1.366±0.558	0.888±0.488	0.197±0.115
15.0	13.8	10.868±0.578	5.916±0.350	2.614±0.227	1.507±0.184	0.639±0.093	0.117±0.021
15.0	29.7	9.970±0.354	5.522±0.208	3.071±0.171	1.489±0.120	0.722±0.070	0.157±0.020
15.0	77.6	10.706±0.643	5.201±0.328	2.540±0.235	1.148±0.158	0.800±0.117	0.194±0.035
17.1	7.8	12.813±1.203	6.744±0.701	2.652±0.420	1.550±0.385	0.783±0.221	0.357±0.157
17.0	13.8	10.060±0.456	5.507±0.275	2.818±0.212	1.576±0.172	0.731±0.087	0.155±0.025
17.0	30.1	10.363±0.390	5.800±0.239	2.914±0.181	1.405±0.123	0.760±0.074	0.144±0.018
17.0	75.6	9.957±0.681	5.230±0.371	2.844±0.295	1.181±0.185	0.641±0.108	0.239±0.044
19.0	7.1	11.642±0.684	6.237±0.392	2.893±0.270	1.706±0.224	0.612±0.091	0.190±0.036
19.0	13.8	10.459±0.460	5.771±0.263	3.196±0.230	1.601±0.157	0.772±0.094	0.195±0.029
18.9	29.9	11.064±0.492	5.521±0.259	2.972±0.203	1.407±0.133	0.762±0.092	0.189±0.031
18.7	66.4	8.940±0.901	5.984±0.612	2.121±0.372	1.786±0.346	1.193±0.246	0.251±0.067

Table 15. $\frac{1}{N_\mu}\cdot\frac{dN^{charged}}{dz}$ in bins of $x(W)$ and Q^2 for the merged data set

Merged data set			dN/dz in bins of x and Q^2 (charged hadrons)				
0.028	2.4	10.086±0.252	5.073±0.118	2.688±0.092	1.461±0.069	0.844±0.046	0.222±0.014
0.029	3.8	10.086±0.254	5.113±0.131	2.587±0.099	1.393±0.077	0.675±0.043	0.191±0.016
0.027	6.4	10.705±0.297	5.392±0.155	2.325±0.110	1.219±0.085	0.574±0.052	0.154±0.020
0.028	9.0	9.842±0.235	5.150±0.136	2.545±0.111	1.207±0.077	0.578±0.045	0.162±0.017
0.031	12.1	9.665±0.348	5.378±0.220	3.438±0.248	1.658±0.177	0.830±0.114	0.253±0.044
0.050	2.5	11.607±0.558	5.329±0.194	2.885±0.136	1.481±0.089	0.803±0.057	0.250±0.019
0.058	3.8	10.170±0.189	5.519±0.090	2.717±0.060	1.502±0.044	0.719±0.024	0.217±0.008
0.060	6.1	10.489±0.170	5.548±0.085	2.670±0.060	1.484±0.045	0.723±0.025	0.188±0.008
0.057	9.4	11.173±0.225	5.892±0.118	2.738±0.080	1.362±0.057	0.678±0.034	0.173±0.010
0.061	13.2	10.540±0.185	5.431±0.102	2.689±0.078	1.482±0.061	0.667±0.033	0.154±0.010
0.067	20.2	10.372±0.150	5.484±0.087	2.715±0.069	1.358±0.050	0.691±0.031	0.154±0.009
0.082	33.1	10.642±0.619	5.290±0.340	2.951±0.307	1.020±0.156	0.671±0.137	0.109±0.033
0.102	4.4	10.046±0.894	5.762±0.373	3.027±0.232	1.736±0.170	0.730±0.075	0.263±0.030
0.122	6.2	11.093±0.406	5.867±0.174	2.897±0.108	1.696±0.079	0.840±0.044	0.220±0.013
0.133	9.1	11.486±0.301	5.874±0.132	2.842±0.085	1.528±0.060	0.741±0.033	0.192±0.010
0.121	13.5	10.908±0.297	5.588±0.141	2.769±0.097	1.463±0.068	0.696±0.036	0.158±0.010
0.139	21.6	10.887±0.156	5.775±0.082	2.776±0.058	1.407±0.040	0.680±0.022	0.159±0.007
0.141	37.2	10.948±0.174	5.652±0.095	2.686±0.068	1.375±0.048	0.690±0.028	0.149±0.008
0.164	61.3	9.499±0.326	4.968±0.184	2.550±0.142	1.356±0.019	0.715±0.065	0.196±0.021
0.226	9.6	10.887±1.269	5.666±0.471	2.882±0.314	1.640±0.225	0.759±0.120	0.264±0.045
0.261	13.4	11.076±0.651	6.601±0.321	3.387±0.215	1.893±0.154	0.819±0.075	0.192±0.020
0.255	24.0	11.181±0.334	6.060±0.159	2.906±0.105	1.589±0.074	0.746±0.039	0.181±0.012
0.269	38.1	10.818±0.255	5.973±0.131	2.900±0.089	1.522±0.063	0.745±0.037	0.144±0.009
0.279	66.2	10.800±0.242	5.767±0.129	2.779±0.089	1.414±0.063	0.701±0.036	0.161±0.011
0.324	118.7	8.990±0.617	4.271±0.313	2.137±0.226	1.266±0.174	0.695±0.106	0.182±0.032
0.472	22.8	9.655±1.351	7.466±0.828	3.607±0.528	1.928±0.351	1.418±0.327	0.301±0.084
0.488	43.2	10.713±1.028	7.269±0.588	3.349±0.364	1.656±0.231	1.314±0.195	0.144±0.040
0.498	69.4	12.613±0.656	6.245±0.300	3.409±0.218	1.664±0.154	0.772±0.082	0.182±0.024
0.525	134.8	10.927±0.713	4.632±0.323	2.488±0.245	1.848±0.209	0.711±0.100	0.202±0.034

Merged data set			dN/dz in bins of W and Q^2 (charged hadrons)				
$\langle W\rangle$	$\langle Q^2\rangle$	$0.10<z<0.15$	$0.15<z<0.25$	$0.25<z<0.35$	$0.35<z<0.45$	$0.45<z<0.60$	$0.60<z<1.0$
7.0	2.9	11.078±0.421	5.556±0.160	2.940±0.108	1.473±0.067	0.764±0.039	0.253±0.015
7.0	6.1	11.086±0.282	5.729±0.117	2.830±0.073	1.661±0.054	0.787±0.029	0.211±0.009
7.1	13.6	10.690±0.390	6.151±0.188	2.958±0.119	1.673±0.087	0.734±0.044	0.205±0.014
7.1	32.8	10.342±0.545	5.998±0.270	2.931±0.172	1.364±0.114	0.855±0.076	0.156±0.019
7.3	72.1	13.373±1.376	5.730±0.549	3.463±0.435	2.152±0.337	0.904±0.183	0.203±0.052
9.0	2.8	10.203±0.210	5.252±0.097	2.606±0.069	1.454±0.052	0.830±0.034	0.216±0.010
9.0	6.4	10.610±0.180	5.553±0.084	2.747±0.058	1.500±0.043	0.706±0.023	0.187±0.007
9.3	14.7	10.834±0.291	5.629±0.136	2.582±0.085	1.478±0.064	0.632±0.031	0.160±0.010
9.3	29.5	11.033±0.329	6.264±0.170	2.871±0.107	1.673±0.081	0.771±0.043	0.174±0.012
9.1	69.5	10.159±0.602	5.395±0.291	2.703±0.205	1.507±0.156	0.698±0.080	0.172±0.024
10.5	2.9	9.932±0.238	5.125±0.124	2.758±0.100	1.504±0.078	0.715±0.043	0.216±0.016
10.8	6.8	10.715±0.177	5.427±0.089	2.663±0.064	1.424±0.049	0.731±0.028	0.191±0.009
10.9	14.1	11.191±0.299	5.692±0.147	2.774±0.103	1.469±0.075	0.666±0.038	0.171±0.012
11.0	29.4	10.847±0.236	5.807±0.121	2.935±0.088	1.411±0.057	0.661±0.031	0.135±0.008
11.1	79.2	10.616±0.423	5.797±0.221	2.862±0.151	1.486±0.111	0.701±0.059	0.127±0.015
12.7	3.6	9.462±0.643	5.398±0.393	2.102±0.253	1.129±0.227	0.614±0.139	0.144±0.041
13.1	6.7	10.395±0.274	5.596±0.147	2.749±0.109	1.472±0.086	0.609±0.045	0.178±0.016
12.9	14.2	10.607±0.277	5.593±0.149	2.732±0.109	1.373±0.074	0.737±0.049	0.169±0.014
13.0	29.1	11.365±0.217	5.946±0.116	2.775±0.079	1.378±0.053	0.753±0.033	0.152±0.009
12.9	70.4	10.733±0.365	5.722±0.193	2.619±0.128	1.398±0.094	0.643±0.051	0.168±0.016
15.0	7.6	10.548±0.326	5.883±0.193	2.652±0.136	1.323±0.102	0.668±0.061	0.171±0.021
15.0	13.9	10.867±0.245	5.669±0.136	2.761±0.101	1.337±0.069	0.653±0.041	0.136±0.011
15.1	29.5	10.851±0.210	5.840±0.118	3.026±0.092	1.539±0.066	0.719±0.036	0.164±0.011
14.9	79.9	11.188±0.390	5.455±0.204	2.818±0.148	1.410±0.104	0.772±0.065	0.191±0.019
17.1	7.8	10.315±0.335	5.286±0.186	2.464±0.146	1.134±0.099	0.587±0.065	0.176±0.028
17.0	13.8	10.185±0.228	5.343±0.132	2.695±0.106	1.430±0.081	0.666±0.046	0.161±0.015
16.9	30.3	10.186±0.215	5.422±0.124	2.481±0.090	1.275±0.065	0.685±0.041	0.147±0.011
17.0	77.6	9.203±0.363	4.628±0.195	2.491±0.154	1.089±0.102	0.610±0.062	0.192±0.021
19.0	7.2	10.978±0.465	6.070±0.287	2.927±0.215	1.684±0.182	0.667±0.087	0.199±0.034
18.8	13.3	9.882±0.240	5.189±0.141	2.924±0.135	1.553±0.106	0.672±0.057	0.207±0.025
19.0	29.4	11.220±0.289	5.624±0.163	2.734±0.131	1.364±0.095	0.756±0.068	0.171±0.022
19.0	66.6	9.444±0.542	5.113±0.320	2.384±0.243	1.819±0.239	0.924±0.145	0.188±0.039

Table 16a. $\frac{1}{N_\mu}\cdot\frac{dN^{charged}}{dp_t}$ in bins of z and W^2 for the merged data set

$0.1<z<0.2$		$0.2<z<0.4$		$0.4<z<1.0$	
p_t^2 [GeV^2]	$\frac{1}{dN_\mu}\frac{dN_h}{dp_t^2}$[GeV^{-2}]	p_t^2 [GeV^2]	$\frac{1}{dN_\mu}\frac{dN_h}{dp_t^2}$[GeV^{-2}]	p_t^2 [GeV^2]	$\frac{1}{dN_\mu}\frac{dN_h}{dp_t^2}$[GeV^{-2}]
$W^2<90$ GeV^2, $\langle W^2\rangle=59.4$ GeV^2					
$0.756\cdot10^{-1}$	$(0.293\pm0.003)\cdot10^{+1}$	$0.813\cdot10^{-1}$	$(0.170\pm0.002)\cdot10^{+1}$	$0.845\cdot10^{-1}$	$(0.562\pm0.010)\cdot10^{+0}$
$0.265\cdot10^{+0}$	$(0.975\pm0.021)\cdot10^{+0}$	$0.267\cdot10^{+0}$	$(0.738\pm0.013)\cdot10^{+0}$	$0.272\cdot10^{+0}$	$(0.336\pm0.008)\cdot10^{+0}$
$0.456\cdot10^{+0}$	$(0.347\pm0.015)\cdot10^{-0}$	$0.457\cdot10^{+0}$	$(0.342\pm0.010)\cdot10^{-0}$	$0.460\cdot10^{+0}$	$(0.187\pm0.006)\cdot10^{-0}$
$0.645\cdot10^{+0}$	$(0.151\pm0.011)\cdot10^{-0}$	$0.645\cdot10^{+0}$	$(0.165\pm0.007)\cdot10^{-0}$	$0.647\cdot10^{+0}$	$(0.116\pm0.005)\cdot10^{-0}$
$0.833\cdot10^{+0}$	$(0.756\pm0.097)\cdot10^{-1}$	$0.833\cdot10^{+0}$	$(0.933\pm0.059)\cdot10^{-1}$	$0.834\cdot10^{+0}$	$(0.705\pm0.040)\cdot10^{-1}$
$0.102\cdot10^{+1}$	$(0.305\pm0.062)\cdot10^{-1}$	$0.102\cdot10^{+1}$	$(0.435\pm0.039)\cdot10^{-1}$	$0.102\cdot10^{+1}$	$(0.427\pm0.030)\cdot10^{-1}$
$0.121\cdot10^{+1}$	$(0.254\pm0.081)\cdot10^{-1}$	$0.121\cdot10^{+1}$	$(0.271\pm0.031)\cdot10^{-1}$	$0.121\cdot10^{+1}$	$(0.248\pm0.022)\cdot10^{-1}$
$0.139\cdot10^{+1}$	$(0.119\pm0.054)\cdot10^{-1}$	$0.140\cdot10^{+1}$	$(0.176\pm0.029)\cdot10^{-1}$	$0.140\cdot10^{+1}$	$(0.226\pm0.026)\cdot10^{-1}$
$0.170\cdot10^{+1}$	$(0.577\pm0.275)\cdot10^{-2}$	$0.171\cdot10^{+1}$	$(0.810\pm0.120)\cdot10^{-2}$	$0.172\cdot10^{+1}$	$(0.962\pm0.089)\cdot10^{-2}$
$0.235\cdot10^{+1}$	$(0.259\pm0.225)\cdot10^{-3}$	$0.237\cdot10^{+1}$	$(0.187\pm0.044)\cdot10^{-2}$	$0.238\cdot10^{+1}$	$(0.189\pm0.023)\cdot10^{-2}$
		$0.341\cdot10^{+1}$	$(0.355\pm0.196)\cdot10^{-3}$	$0.333\cdot10^{+1}$	$(0.581\pm0.126)\cdot10^{-3}$
		$0.461\cdot10^{+1}$	$(0.110\pm0.075)\cdot10^{-3}$	$0.450\cdot10^{+1}$	$(0.177\pm0.068)\cdot10^{-3}$
				$0.628\cdot10^{+1}$	$(0.419\pm0.252)\cdot10^{-4}$
90 GeV$^2<W^2<150$ GeV^2, $\langle W^2\rangle=113.8$ GeV^2					
$0.773\cdot10^{-1}$	$(0.278\pm0.003)\cdot10^{+1}$	$0.817\cdot10^{-1}$	$(0.149\pm0.002)\cdot10^{+1}$	$0.855\cdot10^{-1}$	$(0.439\pm0.011)\cdot10^{-0}$
$0.267\cdot10^{+0}$	$(0.102\pm0.002)\cdot10^{+1}$	$0.269\cdot10^{+0}$	$(0.722\pm0.015)\cdot10^{-0}$	$0.273\cdot10^{+0}$	$(0.274\pm0.009)\cdot10^{-0}$
$0.457\cdot10^{+0}$	$(0.409\pm0.013)\cdot10^{-0}$	$0.457\cdot10^{+0}$	$(0.368\pm0.011)\cdot10^{-0}$	$0.460\cdot10^{+0}$	$(0.173\pm0.007)\cdot10^{-0}$
$0.647\cdot10^{+0}$	$(0.202\pm0.010)\cdot10^{-0}$	$0.647\cdot10^{+0}$	$(0.192\pm0.008)\cdot10^{-0}$	$0.648\cdot10^{+0}$	$(0.124\pm0.007)\cdot10^{-0}$
$0.834\cdot10^{+0}$	$(0.110\pm0.009)\cdot10^{-0}$	$0.834\cdot10^{+0}$	$(0.109\pm0.006)\cdot10^{-0}$	$0.835\cdot10^{+0}$	$(0.782\pm0.051)\cdot10^{-1}$
$0.102\cdot10^{+1}$	$(0.620\pm0.074)\cdot10^{-1}$	$0.102\cdot10^{+1}$	$(0.651\pm0.051)\cdot10^{-1}$	$0.103\cdot10^{+1}$	$(0.510\pm0.044)\cdot10^{-1}$
$0.121\cdot10^{+1}$	$(0.312\pm0.052)\cdot10^{-1}$	$0.121\cdot10^{+1}$	$(0.417\pm0.044)\cdot10^{-1}$	$0.121\cdot10^{+1}$	$(0.374\pm0.038)\cdot10^{-1}$
$0.139\cdot10^{+1}$	$(0.277\pm0.066)\cdot10^{-1}$	$0.140\cdot10^{+1}$	$(0.257\pm0.031)\cdot10^{-1}$	$0.140\cdot10^{+1}$	$(0.242\pm0.027)\cdot10^{-1}$
$0.172\cdot10^{+1}$	$(0.132\pm0.032)\cdot10^{-1}$	$0.174\cdot10^{+1}$	$(0.179\pm0.022)\cdot10^{-1}$	$0.173\cdot10^{+1}$	$(0.156\pm0.016)\cdot10^{-1}$
$0.243\cdot10^{+1}$	$(0.292\pm0.119)\cdot10^{-2}$	$0.242\cdot10^{+1}$	$(0.728\pm0.129)\cdot10^{-2}$	$0.242\cdot10^{+1}$	$(0.648\pm0.092)\cdot10^{-2}$
		$0.339\cdot10^{+1}$	$(0.162\pm0.049)\cdot10^{-2}$	$0.341\cdot10^{+1}$	$(0.151\pm0.025)\cdot10^{-2}$
		$0.466\cdot10^{+1}$	$(0.247\pm0.120)\cdot10^{-3}$	$0.451\cdot10^{+1}$	$(0.509\pm0.115)\cdot10^{-3}$
		$0.652\cdot10^{+1}$	$(0.562\pm0.329)\cdot10^{-4}$	$0.679\cdot10^{+1}$	$(0.171\pm0.053)\cdot10^{-3}$
				$0.983\cdot10^{+1}$	$(0.896\pm0.366)\cdot10^{-5}$
150 GeV$^2<W^2<200$ GeV^2, $\langle W^2\rangle=174.3$ GeV^2					
$0.776\cdot10^{-1}$	$(0.275\pm0.004)\cdot10^{+1}$	$0.818\cdot10^{-1}$	$(0.142\pm0.003)\cdot10^{+1}$	$0.857\cdot10^{-1}$	$(0.373\pm0.027)\cdot10^{-0}$
$0.268\cdot10^{+0}$	$(0.108\pm0.003)\cdot10^{+1}$	$0.270\cdot10^{+0}$	$(0.787\pm0.028)\cdot10^{-0}$	$0.274\cdot10^{+0}$	$(0.252\pm0.015)\cdot10^{-0}$
$0.457\cdot10^{+0}$	$(0.427\pm0.020)\cdot10^{-0}$	$0.459\cdot10^{+0}$	$(0.394\pm0.019)\cdot10^{-0}$	$0.461\cdot10^{+0}$	$(0.166\pm0.012)\cdot10^{-0}$
$0.647\cdot10^{+0}$	$(0.204\pm0.014)\cdot10^{-0}$	$0.647\cdot10^{+0}$	$(0.210\pm0.014)\cdot10^{-0}$	$0.649\cdot10^{+0}$	$(0.110\pm0.010)\cdot10^{-0}$
$0.834\cdot10^{+0}$	$(0.122\pm0.013)\cdot10^{-0}$	$0.837\cdot10^{+0}$	$(0.130\pm0.012)\cdot10^{-0}$	$0.838\cdot10^{+0}$	$(0.865\pm0.093)\cdot10^{-1}$
$0.103\cdot10^{+1}$	$(0.648\pm0.090)\cdot10^{-1}$	$0.103\cdot10^{+1}$	$(0.652\pm0.076)\cdot10^{-1}$	$0.102\cdot10^{+1}$	$(0.497\pm0.058)\cdot10^{-1}$
$0.121\cdot10^{+1}$	$(0.401\pm0.071)\cdot10^{-1}$	$0.122\cdot10^{+1}$	$(0.566\pm0.085)\cdot10^{-1}$	$0.121\cdot10^{+1}$	$(0.411\pm0.067)\cdot10^{-1}$
$0.140\cdot10^{+1}$	$(0.257\pm0.059)\cdot10^{-1}$	$0.140\cdot10^{+1}$	$(0.342\pm0.066)\cdot10^{-1}$	$0.140\cdot10^{+1}$	$(0.238\pm0.044)\cdot10^{-1}$
$0.174\cdot10^{+1}$	$(0.122\pm0.026)\cdot10^{-1}$	$0.174\cdot10^{+1}$	$(0.198\pm0.029)\cdot10^{-1}$	$0.175\cdot10^{+1}$	$(0.180\pm0.023)\cdot10^{-1}$
$0.242\cdot10^{+1}$	$(0.438\pm0.159)\cdot10^{-2}$	$0.245\cdot10^{+1}$	$(0.775\pm0.140)\cdot10^{-2}$	$0.244\cdot10^{+1}$	$(0.782\pm0.140)\cdot10^{-2}$
$0.338\cdot10^{+1}$	$(0.859\pm0.621)\cdot10^{-3}$	$0.345\cdot10^{+1}$	$(0.257\pm0.073)\cdot10^{-2}$	$0.339\cdot10^{+1}$	$(0.225\pm0.055)\cdot10^{-2}$
		$0.457\cdot10^{+1}$	$(0.458\pm0.187)\cdot10^{-3}$	$0.465\cdot10^{+1}$	$(0.128\pm0.044)\cdot10^{-2}$
		$0.660\cdot10^{+1}$	$(0.155\pm0.087)\cdot10^{-3}$	$0.670\cdot10^{+1}$	$(0.246\pm0.086)\cdot10^{-3}$
				$0.974\cdot10^{+1}$	$(0.212\pm0.197)\cdot10^{-3}$
				$0.137\cdot10^{+2}$	$(0.846\pm0.359)\cdot10^{-5}$

Table 16b. $\frac{1}{N_\mu}\cdot\frac{dN^{charged}}{dp_t}$ in bins of z and W^2 for the merged data set

$0.1<z<0.2$		$0.2<z<0.4$		$0.4<z<1.0$	
p_t^2 [GeV^2]	$\frac{1}{dN_\mu}\frac{dN_h}{dp_t^2}$ [GeV^{-2}]	p_t^2 [GeV^2]	$\frac{1}{dN_\mu}\frac{dN_\mu}{dp_t^2}$ [GeV^{-2}]	p_t^2 [GeV^2]	$\frac{1}{dN_\mu}\frac{dN_h}{dp_t^2}$ [GeV^{-2}]
$200\ \text{GeV}^2<W^2<275\ \text{GeV}^2$, $\langle W^2\rangle=236\ \text{GeV}^2$					
$0.785\cdot10^{-1}$	$(0.255\pm0.003)\cdot10^{+1}$	$0.827\cdot10^{-1}$	$(0.132\pm0.003)\cdot10^{+1}$	$0.853\cdot10^{-1}$	$(0.326\pm0.014)\cdot10^{-0}$
$0.267\cdot10^{+0}$	$(0.965\pm0.022)\cdot10^{-0}$	$0.270\cdot10^{+0}$	$(0.725\pm0.022)\cdot10^{-0}$	$0.273\cdot10^{+0}$	$(0.223\pm0.013)\cdot10^{-0}$
$0.458\cdot10^{+0}$	$(0.420\pm0.015)\cdot10^{-0}$	$0.458\cdot10^{+0}$	$(0.357\pm0.015)\cdot10^{-0}$	$0.461\cdot10^{+0}$	$(0.150\pm0.010)\cdot10^{-0}$
$0.646\cdot10^{+0}$	$(0.237\pm0.012)\cdot10^{-0}$	$0.647\cdot10^{+0}$	$(0.209\pm0.012)\cdot10^{-0}$	$0.648\cdot10^{+0}$	$(0.990\pm0.084)\cdot10^{-1}$
$0.837\cdot10^{+0}$	$(0.127\pm0.009)\cdot10^{-0}$	$0.836\cdot10^{+0}$	$(0.127\pm0.009)\cdot10^{-0}$	$0.837\cdot10^{+0}$	$(0.658\pm0.062)\cdot10^{-1}$
$0.102\cdot10^{+1}$	$(0.681\pm0.063)\cdot10^{-1}$	$0.103\cdot10^{+1}$	$(0.885\pm0.084)\cdot10^{-1}$	$0.102\cdot10^{+1}$	$(0.608\pm0.075)\cdot10^{-1}$
$0.121\cdot10^{+1}$	$(0.496\pm0.058)\cdot10^{-1}$	$0.121\cdot10^{+1}$	$(0.521\pm0.059)\cdot10^{-1}$	$0.121\cdot10^{+1}$	$(0.383\pm0.055)\cdot10^{-1}$
$0.140\cdot10^{+1}$	$(0.294\pm0.043)\cdot10^{-1}$	$0.140\cdot10^{+1}$	$(0.407\pm0.049)\cdot10^{-1}$	$0.140\cdot10^{+1}$	$(0.281\pm0.042)\cdot10^{-1}$
$0.173\cdot10^{+1}$	$(0.182\pm0.023)\cdot10^{-1}$	$0.174\cdot10^{+1}$	$(0.203\pm0.021)\cdot10^{-1}$	$0.172\cdot10^{+1}$	$(0.179\pm0.022)\cdot10^{-1}$
$0.242\cdot10^{+1}$	$(0.507\pm0.084)\cdot10^{-2}$	$0.246\cdot10^{+1}$	$(0.746\pm0.090)\cdot10^{-2}$	$0.244\cdot10^{+1}$	$(0.735\pm0.097)\cdot10^{-2}$
$0.337\cdot10^{+1}$	$(0.171\pm0.050)\cdot10^{-2}$	$0.342\cdot10^{+1}$	$(0.174\pm0.034)\cdot10^{-2}$	$0.341\cdot10^{+1}$	$(0.314\pm0.052)\cdot10^{-2}$
$0.461\cdot10^{+1}$	$(0.607\pm0.278)\cdot10^{-3}$	$0.462\cdot10^{+1}$	$(0.105\pm0.024)\cdot10^{-2}$	$0.462\cdot10^{+1}$	$(0.136\pm0.027)\cdot10^{-2}$
$0.669\cdot10^{+1}$	$(0.605\pm0.439)\cdot10^{-4}$	$0.690\cdot10^{+1}$	$(0.338\pm0.111)\cdot10^{-3}$	$0.680\cdot10^{+1}$	$(0.383\pm0.094)\cdot10^{-3}$
		$0.102\cdot10^{+2}$	$(0.174\pm0.098)\cdot10^{-3}$	$0.986\cdot10^{+1}$	$(0.259\pm0.145)\cdot10^{-3}$
		$0.145\cdot10^{+2}$	$(0.146\pm0.102)\cdot10^{-4}$	$0.137\cdot10^{+2}$	$(0.709\pm0.396)\cdot10^{-4}$
$275\ \text{GeV}^2<W^2<350\ \text{GeV}^2$, $\langle W^2\rangle=310.9\ \text{GeV}^2$					
$0.778\cdot10^{-1}$	$(0.235\pm0.004)\cdot10^{+1}$	$0.823\cdot10^{-1}$	$(0.120\pm0.003)\cdot10^{+1}$	$0.865\cdot10^{-1}$	$(0.320\pm0.019)\cdot10^{-0}$
$0.268\cdot10^{+0}$	$(0.938\pm0.026)\cdot10^{-0}$	$0.269\cdot10^{+0}$	$(0.692\pm0.027)\cdot10^{-0}$	$0.272\cdot10^{+0}$	$(0.210\pm0.017)\cdot10^{-0}$
$0.458\cdot10^{+0}$	$(0.392\pm0.016)\cdot10^{-0}$	$0.459\cdot10^{+0}$	$(0.337\pm0.017)\cdot10^{-0}$	$0.461\cdot10^{+0}$	$(0.136\pm0.012)\cdot10^{-0}$
$0.645\cdot10^{+0}$	$(0.212\pm0.012)\cdot10^{-0}$	$0.647\cdot10^{+0}$	$(0.200\pm0.014)\cdot10^{-0}$	$0.648\cdot10^{+0}$	$(0.853\pm0.094)\cdot10^{-1}$
$0.837\cdot10^{+0}$	$(0.120\pm0.009)\cdot10^{-0}$	$0.834\cdot10^{+0}$	$(0.140\pm0.012)\cdot10^{-0}$	$0.840\cdot10^{+0}$	$(0.669\pm0.086)\cdot10^{-1}$
$0.102\cdot10^{+1}$	$(0.713\pm0.071)\cdot10^{-1}$	$0.103\cdot10^{+1}$	$(0.811\pm0.088)\cdot10^{-1}$	$0.103\cdot10^{+1}$	$(0.507\pm0.074)\cdot10^{-1}$
$0.121\cdot10^{+1}$	$(0.434\pm0.052)\cdot10^{-1}$	$0.131\cdot10^{+1}$	$(0.495\pm0.067)\cdot10^{-1}$	$0.121\cdot10^{+1}$	$(0.358\pm0.059)\cdot10^{-1}$
$0.140\cdot10^{+1}$	$(0.348\pm0.048)\cdot10^{-1}$	$0.140\cdot10^{+1}$	$(0.323\pm0.045)\cdot10^{-1}$	$0.140\cdot10^{+1}$	$(0.251\pm0.049)\cdot10^{-1}$
$0.173\cdot10^{+1}$	$(0.160\pm0.018)\cdot10^{-1}$	$0.176\cdot10^{+1}$	$(0.199\pm0.025)\cdot10^{-1}$	$0.173\cdot10^{+1}$	$(0.196\pm0.028)\cdot10^{-1}$
$0.244\cdot10^{+1}$	$(0.670\pm0.104)\cdot10^{-2}$	$0.246\cdot10^{+1}$	$(0.821\pm0.105)\cdot10^{-2}$	$0.245\cdot10^{+1}$	$(0.713\pm0.121)\cdot10^{-2}$
$0.338\cdot10^{+1}$	$(0.251\pm0.059)\cdot10^{-2}$	$0.342\cdot10^{+1}$	$(0.255\pm0.047)\cdot10^{-2}$	$0.345\cdot10^{+1}$	$(0.547\pm0.124)\cdot10^{-2}$
$0.470\cdot10^{+1}$	$(0.554\pm0.187)\cdot10^{-3}$	$0.468\cdot10^{+1}$	$(0.157\pm0.035)\cdot10^{-2}$	$0.465\cdot10^{+1}$	$(0.151\pm0.036)\cdot10^{-2}$
$0.666\cdot10^{+1}$	$(0.138\pm0.085)\cdot10^{-3}$	$0.679\cdot10^{+1}$	$(0.433\pm0.110)\cdot10^{-3}$	$0.678\cdot10^{+1}$	$(0.531\pm0.137)\cdot10^{-3}$
$0.101\cdot10^{+2}$	$(0.276\pm0.260)\cdot10^{-4}$	$0.996\cdot10^{+1}$	$(0.825\pm0.439)\cdot10^{-4}$	$0.975\cdot10^{+1}$	$(0.775\pm0.210)\cdot10^{-4}$
		$0.158\cdot10^{+2}$	$(0.895\pm0.736)\cdot10^{-5}$	$0.147\cdot10^{+2}$	$(0.489\pm0.156)\cdot10^{-4}$
$350\ \text{GeV}^2<W^2$, $\langle W^2\rangle=389.9\ \text{GeV}^2$					
$0.780\cdot10^{-1}$	$(0.236\pm0.004)\cdot10^{+1}$	$0.819\cdot10^{-1}$	$(0.125\pm0.004)\cdot10^{+1}$	$0.853\cdot10^{-1}$	$(0.367\pm0.024)\cdot10^{-0}$
$0.268\cdot10^{+0}$	$(0.928\pm0.027)\cdot10^{-0}$	$0.271\cdot10^{+0}$	$(0.696\pm0.030)\cdot10^{-0}$	$0.273\cdot10^{+0}$	$(0.232\pm0.021)\cdot10^{-0}$
$0.457\cdot10^{+0}$	$(0.391\pm0.016)\cdot10^{-0}$	$0.459\cdot10^{+0}$	$(0.366\pm0.021)\cdot10^{-0}$	$0.462\cdot10^{+0}$	$(0.146\pm0.016)\cdot10^{-0}$
$0.645\cdot10^{+0}$	$(0.219\pm0.012)\cdot10^{-0}$	$0.647\cdot10^{+0}$	$(0.209\pm0.016)\cdot10^{-0}$	$0.651\cdot10^{+0}$	$(0.125\pm0.016)\cdot10^{-0}$
$0.837\cdot10^{+0}$	$(0.119\pm0.009)\cdot10^{-0}$	$0.835\cdot10^{+0}$	$(0.125\pm0.011)\cdot10^{-0}$	$0.840\cdot10^{+0}$	$(0.751\pm0.115)\cdot10^{-1}$
$0.102\cdot10^{+1}$	$(0.782\pm0.072)\cdot10^{-1}$	$0.103\cdot10^{+1}$	$(0.836\pm0.103)\cdot10^{-1}$	$0.102\cdot10^{+1}$	$(0.811\pm0.158)\cdot10^{-1}$
$0.121\cdot10^{+1}$	$(0.554\pm0.064)\cdot10^{-1}$	$0.121\cdot10^{+1}$	$(0.693\pm0.096)\cdot10^{-1}$	$0.121\cdot10^{+1}$	$(0.598\pm0.133)\cdot10^{-1}$
$0.140\cdot10^{+1}$	$(0.369\pm0.045)\cdot10^{-1}$	$0.140\cdot10^{+1}$	$(0.398\pm0.063)\cdot10^{-1}$	$0.140\cdot10^{+1}$	$(0.255\pm0.064)\cdot10^{-1}$
$0.174\cdot10^{+1}$	$(0.194\pm0.020)\cdot10^{-1}$	$0.174\cdot10^{+1}$	$(0.235\pm0.028)\cdot10^{-1}$	$0.174\cdot10^{+1}$	$(0.247\pm0.045)\cdot10^{-1}$
$0.243\cdot10^{+1}$	$(0.743\pm0.100)\cdot10^{-2}$	$0.246\cdot10^{+1}$	$(0.975\pm0.130)\cdot10^{-2}$	$0.246\cdot10^{+1}$	$(0.113\pm0.021)\cdot10^{-1}$
$0.346\cdot10^{+1}$	$(0.281\pm0.062)\cdot10^{-2}$	$0.342\cdot10^{+1}$	$(0.399\pm0.068)\cdot10^{-2}$	$0.340\cdot10^{+1}$	$(0.405\pm0.099)\cdot10^{-2}$
$0.453\cdot10^{+1}$	$(0.118\pm0.026)\cdot10^{-2}$	$0.462\cdot10^{+1}$	$(0.153\pm0.027)\cdot10^{-2}$	$0.467\cdot10^{+1}$	$(0.150\pm0.034)\cdot10^{-2}$
$0.687\cdot10^{+1}$	$(0.243\pm0.113)\cdot10^{-3}$	$0.669\cdot10^{+1}$	$(0.454\pm0.093)\cdot10^{-3}$	$0.677\cdot10^{+1}$	$(0.132\pm0.041)\cdot10^{-2}$
$0.954\cdot10^{+1}$	$(0.262\pm0.223)\cdot10^{-4}$	$0.100\cdot10^{+2}$	$(0.274\pm0.134)\cdot10^{-3}$	$0.104\cdot10^{+2}$	$(0.326\pm0.152)\cdot10^{-3}$
		$0.141\cdot10^{+2}$	$(0.385\pm0.154)\cdot10^{-4}$	$0.138\cdot10^{+2}$	$(0.634\pm0.242)\cdot10^{-4}$

Table 17. W^2 dependence of $\langle p_t^2 \rangle$ in bins of z and Q^2 for the merged data set

Q^2 [GeV^2]	$\langle W^2 \rangle$ [GeV^2]	$\langle p_t^2 \rangle$ [GeV^2]		
		$0.10 < z < 0.20$	$0.20 < z < 0.40$	$0.40 < z < 1.0$
2.0– 5.0	42.2 [30–50]	0.175 ± 0.007	0.256 ± 0.009	0.336 ± 0.014
2.0– 5.0	67.7 [50–90]	0.205 ± 0.003	0.282 ± 0.004	0.386 ± 0.009
2.0– 5.0	103.9 [90–120]	0.234 ± 0.003	0.307 ± 0.005	0.399 ± 0.010
2.0– 5.0	133.8 [120–150]	0.242 ± 0.010	0.325 ± 0.019	0.501 ± 0.056
2.0– 5.0	182.4 [150–200]	0.261 ± 0.029	0.475 ± 0.069	0.544 ± 0.134
2.0– 5.0	235.3 [200–275]	0.297 ± 0.013	0.366 ± 0.024	0.692 ± 0.092
2.0– 5.0	289.5 [275–350]	0.264 ± 0.014	0.394 ± 0.032	0.684 ± 0.136
5.0–10.0	40.4 [30–50]	0.175 ± 0.005	0.226 ± 0.006	0.342 ± 0.012
5.0–10.0	69.5 [50–90]	0.209 ± 0.003	0.288 ± 0.004	0.428 ± 0.009
5.0–10.0	104.8 [90–120]	0.242 ± 0.004	0.340 ± 0.007	0.537 ± 0.017
5.0–10.0	135.3 [120–150]	0.241 ± 0.008	0.353 ± 0.014	0.546 ± 0.038
5.0–10.0	177.7 [150–200]	0.254 ± 0.009	0.357 ± 0.016	0.555 ± 0.043
5.0–10.0	239.9 [200–275]	0.282 ± 0.009	0.403 ± 0.018	0.554 ± 0.045
5.0–10.0	313.3 [275–350]	0.309 ± 0.010	0.407 ± 0.020	0.733 ± 0.069
5.0–10.0	394.1 [350–500]	0.323 ± 0.008	0.428 ± 0.016	0.830 ± 0.056
10.0–20.0	37.5 [30–50]	0.174 ± 0.006	0.236 ± 0.008	0.341 ± 0.017
10.0–20.0	73.1 [50–90]	0.213 ± 0.004	0.282 ± 0.006	0.442 ± 0.013
10.0–20.0	104.4 [90–120]	0.285 ± 0.009	0.367 ± 0.013	0.580 ± 0.030
10.0–20.0	135.0 [120–150]	0.262 ± 0.011	0.348 ± 0.018	0.521 ± 0.042
10.0–20.0	173.9 [150–200]	0.274 ± 0.008	0.401 ± 0.015	0.587 ± 0.036
10.0–20.0	232.4 [200–275]	0.293 ± 0.006	0.402 ± 0.011	0.704 ± 0.031
10.0–20.0	311.8 [275–350]	0.311 ± 0.006	0.433 ± 0.013	0.721 ± 0.038
10.0–20.0	386.9 [350–500]	0.339 ± 0.006	0.466 ± 0.014	0.723 ± 0.040
20.0–40.0	35.0 [30–50]	0.202 ± 0.012	0.234 ± 0.014	0.364 ± 0.031
20.0–40.0	75.8 [50–90]	0.212 ± 0.005	0.259 ± 0.007	0.417 ± 0.017
20.0–40.0	104.0 [90–120]	0.239 ± 0.006	0.327 ± 0.010	0.521 ± 0.024
20.0–40.0	134.2 [120–150]	0.272 ± 0.006	0.351 ± 0.009	0.548 ± 0.022
20.0–40.0	171.9 [150–200]	0.260 ± 0.005	0.356 ± 0.008	0.593 ± 0.021
20.0–40.0	238.4 [200–275]	0.293 ± 0.004	0.396 ± 0.008	0.678 ± 0.024
20.0–40.0	307.7 [275–350]	0.318 ± 0.006	0.422 ± 0.012	0.699 ± 0.034
20.0–40.0	383.9 [350–500]	0.313 ± 0.007	0.477 ± 0.018	0.775 ± 0.056
>40.0	44.3 [30–50]	0.196 ± 0.023	0.261 ± 0.033	0.421 ± 0.077
>40.0	72.1 [50–90]	0.206 ± 0.008	0.272 ± 0.011	0.474 ± 0.030
>40.0	104.1 [90–120]	0.220 ± 0.008	0.325 ± 0.013	0.488 ± 0.030
>40.0	134.8 [120–150]	0.231 ± 0.007	0.319 ± 0.011	0.585 ± 0.033
>40.0	174.2 [150–200]	0.270 ± 0.006	0.359 ± 0.010	0.666 ± 0.030
>40.0	238.5 [200–275]	0.290 ± 0.006	0.410 ± 0.011	0.666 ± 0.030
>40.0	305.2 [275–350]	0.301 ± 0.008	0.429 ± 0.016	0.716 ± 0.040
>40.0	372.4 [350–500]	0.318 ± 0.015	0.453 ± 0.031	0.897 ± 0.107

Table 18. W^2 dependence of $\langle p_t^2 \rangle$ integrated over Q^2 for the merged data set

$\langle W^2 \rangle$ [GeV^2]	$\langle p_t^2 \rangle$ [GeV^2]		
	$0.10 < z < 0.20$	$0.20 < z < 0.40$	$0.40 < z < 1.0$
41.0 [30–50]	0.186 ± 0.004	0.240 ± 0.005	0.336 ± 0.008
69.6 [50–90]	0.206 ± 0.002	0.276 ± 0.003	0.406 ± 0.005
104.2 [90–120]	0.244 ± 0.002	0.341 ± 0.004	0.500 ± 0.009
134.8 [120–150]	0.259 ± 0.004	0.347 ± 0.007	0.549 ± 0.018
174.3 [150–200]	0.267 ± 0.003	0.374 ± 0.006	0.609 ± 0.016
236.0 [200–275]	0.291 ± 0.003	0.399 ± 0.006	0.665 ± 0.016
310.9 [275–350]	0.306 ± 0.004	0.420 ± 0.008	0.719 ± 0.023
389.9 [350–500]	0.323 ± 0.004	0.444 ± 0.009	0.763 ± 0.028

Table 19. Ratio of charge multiplicities in bins of x and z

$\langle z \rangle$	$(dN/dz)^+/(dN/dz)^-$ for $0.01<x<0.02$		
	proton	deuteron	neutron
0.12	1.05±0.18	1.00±0.09	0.94±0.28
0.17	1.17±0.27	1.06±0.14	0.95±0.37
0.22	1.00±0.33	1.01±0.17	1.01±0.38
0.29	1.41±0.41	1.04±0.15	0.79±0.33
0.41	2.75±1.19	1.01±0.18	0.46±0.34
0.63	1.27±0.73	1.88±0.39	2.37±1.16
$\langle z \rangle$	$(dN/dz)^+/(dN/dz)^-$ for $0.02<x<0.035$		
	proton	deuteron	neutron
0.12	1.17±0.04	1.12±0.04	1.06±0.09
0.17	1.21±0.05	1.13±0.05	1.04±0.12
0.22	1.21±0.07	1.13±0.07	1.02±0.17
0.27	1.12±0.08	1.21±0.09	1.33±0.24
0.32	1.16±0.10	1.11±0.10	1.06±0.19
0.37	1.20±0.13	1.21±0.12	1.22±0.26
0.42	1.34±0.17	1.23±0.15	1.13±0.31
0.47	1.30±0.21	1.82±0.24	2.37±0.66
0.52	1.40±0.26	1.75±0.28	2.05±0.64
0.57	1.64±0.35	1.62±0.30	1.59±0.65
0.63	1.62±0.42	1.55±0.31	1.50±0.60
0.68	1.58±0.51	1.34±0.32	1.15±0.65
0.77	1.23±0.29	1.29±0.23	1.34±0.47
0.89	4.21±2.01	1.32±0.38	0.74±0.48
$\langle z \rangle$	$(dN/dz)^+/(dN/dz)^-$ for $0.035<x<0.09$		
	proton	deuteron	neutron
0.12	1.21±0.02	1.15±0.03	1.06±0.07
0.17	1.20±0.03	1.18±0.03	1.16±0.09
0.22	1.23±0.04	1.22±0.04	1.21±0.10
0.27	1.32±0.05	1.35±0.06	1.39±0.14
0.32	1.45±0.07	1.38±0.07	1.31±0.16
0.37	1.42±0.08	1.23±0.07	1.05±0.15
0.42	1.62±0.11	1.48±0.10	1.34±0.21
0.47	1.56±0.13	1.46±0.11	1.35±0.24
0.52	1.41±0.13	1.51±0.13	1.62±0.33
0.57	1.54±0.17	1.39±0.14	1.28±0.27
0.63	1.66±0.22	1.61±0.18	1.57±0.35
0.69	1.99±0.22	1.54±0.14	1.20±0.25
0.80	1.62±0.25	1.45±0.18	1.29±0.39
0.91	2.30±0.51	1.55±0.25	1.26±0.34
$\langle z \rangle$	$(dN/dz)^+/(dN/dz)^-$ for $0.09<x<0.2$		
	proton	deuteron	neutron
0.12	1.20±0.03	1.23±0.04	1.27±0.11
0.17	1.32±0.04	1.21±0.04	1.06±0.11
0.22	1.43±0.05	1.27±0.06	1.04±0.14
0.27	1.42±0.06	1.34±0.07	1.23±0.18
0.32	1.75±0.09	1.30±0.08	0.84±0.14
0.37	1.79±0.11	1.53±0.10	1.24±0.23
0.42	1.87±0.13	1.57±0.12	1.27±0.24
0.47	1.92±0.16	1.59±0.14	1.26±0.29
0.52	2.20±0.19	1.47±0.15	0.79±0.25
0.60	2.36±0.19	2.06±0.18	1.61±0.45
0.69	2.96±0.33	1.68±0.19	0.60±0.29
0.79	3.05±0.46	2.24±0.34	1.55±0.58
0.90	2.15±0.46	2.04±0.42	1.94±0.87
$\langle z \rangle$	$(dN/dz)^+/(dN/dz)^-$ for $0.2<x<0.4$		
	proton	deuteron	neutron
0.12	1.31±0.05	1.31±0.06	1.31±0.18
0.17	1.35±0.06	1.27±0.07	1.13±0.20
0.22	1.50±0.08	1.28±0.08	0.97±0.19
0.27	1.68±0.10	1.27±0.09	0.72±0.20
0.32	1.97±0.14	1.56±0.14	0.96±0.30
0.37	1.99±0.17	1.68±0.17	1.15±0.43
0.42	2.20±0.22	1.88±0.22	1.44±0.51
0.47	2.47±0.29	1.85±0.27	1.02±0.53
0.55	2.60±0.26	1.65±0.19	0.86±0.29
0.64	4.16±0.63	2.29±0.36	1.03±0.47
0.77	4.70±0.88	3.52±0.70	2.49±1.15
0.90	5.02±1.83	3.61±1.25	2.22±2.16
$\langle z \rangle$	$(dN/dz)^+/(dN/dz)^-$ for $0.4<x<0.6$		
	proton	deuteron	neutron
0.12	1.37±0.14	1.38±0.16	1.38±0.66
0.17	1.47±0.18	1.30±0.18	0.97±0.55
0.25	1.85±0.21	1.89±0.25	2.06±1.42
0.39	2.94±0.37	2.10±0.31	0.93±0.60
0.64	4.34±0.96	2.37±0.56	0.15±0.82
$\langle z \rangle$	$(dN/dz)^+/(dN/dz)^-$ for $0.6<x<1.0$		
	proton	deuteon	neutron
0.12	1.45±0.41	1.35±0.58	0.09±6.75
0.19	1.87±0.53	1.05±0.44	0.91±1.67
0.31	2.04±0.86	2.60±1.23	4.35±9.69
0.41	3.47±1.56	2.15±1.05	0.59±1.70
0.64	2.48±1.30	5.47±6.02	0.34±2.26

References

1. M. Gronau, F. Ravndal, Y. Zarmi: Nucl. Phys. B51 (1973) 611
2. EMC. Publications related to forward produced hadrons in deep inelastic muon scattering: J.J. Aubert et al.: Phys. Lett. B95 (1980) 306; J.J. Aubert, et al.: Phys. Lett. B103 (1981) 388; J.J. Aubert et al.: Phys. Lett. B114 (1982) 373; J.J. Aubert et al.: Phys. Lett. B119 (1982) 233; J.J. Aubert et al.: Z. Phys. C – Particles and Fields 18 (1983) 189; J.J. Aubert et al.: Phys. Lett. B130 (1983) 118; J.J. Aubert et al.: Phys. Lett. B133 (1983) 370; J.J. Aubert et al.: Phys. Lett. 135 (1984) 225; A. Arvidson et al.: Nucl. Phys. B246 (1984) 381; J.J. Aubert et al.: Phys. Lett. B160 (1985) 417; J.J. Aubert et al.: Phys. Lett, B161 (1985) 203; J.J. Aubert et al.: Phys. Lett. B165 (1985) 222; J.J. Aubert et al.: Phys. Lett. B167 (1986) 127; J.J. Aubert et al.: Z. Phys. C – Particles and Fields 30 (1986) 23; J.J. Aubert et al.: Z. Phys. C – Particles and Fields 31 (1986) 175; J. Ashman et al.: Z. Phys. C – Particles and Fields 39 (1988) 169; J.J. Aubert et al.: Phys. Lett. B218 (1989) 248
3. Particles Data Group: Phys. Lett. B239 (1990) 48
4. EMC, J.J. Aubert et al.: Phys. Lett. B130 (1983) 118
5. EMC. Publications related to measures of eventshapes in deep inelastic muon scattering: J.J. Aubert et al.: Phys. Lett. B100 (1981) 433; J.P. Albanese et al.: Phys. Lett. B144 (1984) 302; M. Arneodo et al.: Phys. Lett. B149 (1984) 415; M. Arneodo et al.: Z. Phys. C – Particles and Fields 31 (1986) 1; M. Arneodo et al.: Z. Phys. C – Particles and Fields 31 (1986) 333; M. Arneodo et al.: Z. Phys. C – Particles and Fields 35 (1987) 417; M.

Arneodo et al.: Z. Phys. C – Particles and Fields 33 (1987) 277; M. Arneodo et al.: Z. Phys. C – Particles and Fields 36 (1987) 527; M. Arneodo et al.: Z. Phys. C – Particles and Fields 40 (1988) 347; M. Arneodo et al.: Nucl. Phys. B321 (1989) 541
6. A. Bodek, A. Simon: Z. Phys. C – Particles and Fields 29 (1985) 231
7. EMC, J.J. Aubert et al.: Nucl. Phys. B293 (1987) 740. The structure function ratio was parametrized as $F_2^n(x)/F_2^p(x) = 0.947 - 0.930 \cdot x$
8. R. Mount: Proc. XXIV International Conference on High Energy Physics, München (1988) 1007
9. NMC, D. Allasia et al.: Phys. Lett. B249 (1990) 366; NMC, P. Amandruz et al.: CERN preprint, CERN-PPE 91-05 (1991)
10. EMC, J.J. Aubert et al.: Phys. Lett. B160 (1985) 417
11. EMC, O.C. Allkofer et al.: Nucl. Instrum. Methods 179 (1981) 445
12. EMC, J.J. Aubert et al.: Nucl. Phys. B259 (1985) 189
13. EMC, J. Ashman et al.: Nucl. Phys. B328 (1989) 1
14. EMC, J.J. Aubert et al.: Phys. Lett. B123 (1983) 275
15. EMC, J. Ashman et al.: Comparison of forward hadrons produced in muon interactions on nuclear targets and deuterium, CERN preprint in preparation
16. A. Schneider: Ph.D. Thesis, University of Wuppertal WUB-DI 85-7 (1985)
17. B. Korzen: Ph.D. Thesis, University of Wuppertal WUB 89-7 (1989)
18. T. Sjostrand et al.: Comput. Phys. Commun. 27 (1982) 243
19. T. Sjostrand, M. Bengtsson: Lepto 5.2, DESY preprint in preparation
20. T. Sjostrand et al.: Lund University preprint LU-TP 85-10 (1985); Lund University preprint LU-TP 86-22 (1986)
21. L.W. Mo, Y.T. Tsai: Rev. Mod. Phys. 41 (1969) 205; J. Drees: Wuppertal University preprint WUB 78-16 (1978)
22. C.P. Bee: EMC Internal Report 86/8 (1986)
23. U. Krüner: Diplom Thesis, University of Wuppertal WUD 88–27 (1988)
24. EMC, J.J. Aubert et al.: Phys. Lett. B114 (1982) 373
25. EMC, J.J. Aubert et al.: Phys. Lett. B165 (1985) 222
26. EMC, J.J. Aubert et al.: Z. Phys. C – Particles and Fields 30 (1986) 23
27. EMC, J.J. Aubert et al.: Phys. Lett. B95 (1980) 306
28. EMC, M. Arneodo et al.: Z. Phys. C – Particles and Fields 36 (1987) 527
29. H. Deden et al.: Nucl. Phys. B181 (1981) 375
30. EMC, M. Arneodo et al.: Z. Phys. C – Particles and Fields 35 (1987) 417
31. TASSO, R. Brandelik et al.: Phys. Lett. B94 (1980) 437
32. W. Hoffmann: Nucl. Phys. B3 (1988) 671
33. M. Bengtsson: private communication (1988)
34. EMC, M. Arneodo et al.: Z. Phys. C – Particles and Fields 40 (1988) 347
35. CHIO, W.A. Loomis et al.: Phys. Rev. D19 (1979) 2543
36. C.J. Bebek et al.: Phys. Rev. D16 (1977) 1986; I. Dammann et al.: Nucl. Phys. B54 (1973) 381; J.F. Martin et al.: Phys. Lett. B65 (1976) 483; C. del Papa et al.: Phys. Rev. D15 (1977) 2425
37. Dakin et al.: Phys. Rev. D10 (1974) 1401
38. EMC, M. Arneodo et al.: Phys. Lett. B150 (1985) 458
39. W. Hoffmann: Ann. Rev. Nucl. Part. Sci. 38 (1988) 279
40. J. Drees: 1981 International Symposium on Lepton and Photon Interactions at high Energies, Bonn (1981)
41. EMC, J.J. Aubert et al.: Phys. Lett. B161 (1985) 203
42. BEBC, D. Allasia et al.: Phys. Lett. 135 (1984) 231. After the completion of this analysis preliminary results on $d_v(x)/u_v(x)$ have been given by two other BEBC experiments: [.1] G.T. Jones et al.: Contribution to 1989 International Symposium on Lepton and Photon Interactions at High Energies (1989); [.2] G.T. Jones et al.: Oxford University preprint OUNP 89-18 (1989); [.1] agrees with our analysis, whereas the data [.2] are below our data at low x
43. CDHS, H. Abramowicz et al.: Z. Phys. C – Particles and Fields 25 (1984) 29
44. B.L. Ioffe, A.B. Kaidalov: Phys. Lett. B150 (1985) 374
45. R.D. Field, R.P. Feynmann: Phys. Rev. D15 (1977) 2590
46. M. Diemoz, F. Ferroni, E. Longo, G. Martinelli: CERN preprint CERN-TH 4751-87 (1987)
47. A.D. Martin, R.G. Roberts, W.J. Stirling: Phys. Lett. B206 (1988) 327
48. V. Gibson: Ph.D. Thesis, University of Oxford RAL-T-035 (1986)
49. EMC, J.J. Aubert et al.: Nucl. Phys. B293 (1987) 740
50. T. Sloan: Proc. International Europhysics Conference on High Energy Physics (1987)
51. H. Plothow-Besch: PDFLIB: Structure Function and α_s Calculation Users Manual, CERN Program Library W5051